



ATLAS: a rationally designed anterograde transsynaptic tracer

Received: 16 February 2024

Accepted: 11 March 2025

Published online: 1 May 2025

 Check for updates

Jacqueline F. Rivera^{1,7}, Haoyang Huang^{1,2,7}, Weiguang Weng¹, Heesung Sohn^{1,2}, Allison E. Girasole³, Shun Li³, Madeline A. Albanese³, Melissa Qin¹, Can Tao⁴, Molly E. Klug¹, Sadhna Rao^{1,2}, Ronald Paletski⁵, Bruce E. Herring^{1,2}, Scott E. Kanoski^{1,2}, Li I. Zhang⁴, Charles R. Gerfen⁵, Bernardo L. Sabatini³ & Don B. Arnold^{1,2,6} 

Genetically modified rabies virus can map neural circuits retrogradely from genetically determined cells. However, similar tools for anterograde tracing are not available. Here, we describe a method for anterograde transsynaptic tracing from genetically determined neurons based on a rationally designed protein, ATLAS. Expression of ATLAS in neurons causes presynaptic release of a payload composed of an antibody-like protein, AMPA.FingR, which binds to the N terminus of GluA1, and a recombinase. In the synaptic cleft, AMPA.FingR binds to GluA1, causing the payload to be endocytosed into postsynaptic cells and delivered to the nucleus, where it triggers expression of a recombinase-dependent reporter. In mice, ATLAS mediates monosynaptic transneuronal tracing from random or genetically determined cells that is strictly anterograde, synaptic and nontoxic. Moreover, ATLAS-mediated tracing shows activity dependence, suggesting that it can label active circuits underlying specific behaviors. Finally, ATLAS is composed of modular components that can be independently replaced or modified.

Neural circuits underlying sleep¹, interoception², tactile sensory processing³, sexual behavior⁴, digestion⁵ and parenting⁶ have been studied by identifying critical cellular components using activity-dependent reporters and activating those cells optogenetically or through sensory stimulation. However, fully defining the anatomy and function of these circuits requires the identification of cells upstream and downstream of starter cells. This task is difficult due to the heterogeneity of cell types present in relatively small volumes of neural tissue⁷. Thus, classical tracing methods using proteins such as wheat germ agglutinin and horse radish peroxidase⁸, which are taken up by most neurons, cannot be used to define most neuronal circuits precisely.

A genetically modified form of rabies virus was developed that specifically infects neurons expressing the Avian sarcoma leucosis virus receptor, TVA, enabling tracing from specific cell types⁹. Neural circuits carry information from presynaptic to postsynaptic cells, or anterogradely, but modified rabies virus infects neurons that are presynaptic to starter neurons, traveling retrogradely¹⁰. In addition, it is engineered to jump a single synapse, allowing for precise mapping^{11,12}. Although modified rabies virus has been broadly used for tracing circuits retrogradely¹³, there is currently no comparable method for tracing circuits from genetically determined cells anterogradely. In particular, although two viruses have recently been used for anterograde

¹Department of Biological Sciences, Dornsife College, University of Southern California, Los Angeles, CA, USA. ²Neuroscience Graduate Program, University of Southern California, Los Angeles, CA, USA. ³Howard Hughes Medical Institute, Department of Neurobiology, Harvard Medical School, Boston, MA, USA. ⁴Center for Neural Circuits and Sensory Processing Disorders, Zilkha Neurogenetic Institute, Department of Physiology and Neuroscience, Keck School of Medicine, University of Southern California, Los Angeles, CA, USA. ⁵Section on Neuroanatomy, National Institute of Mental Health, Bethesda, MD, USA. ⁶Department of Biomedical Engineering, Viterbi School of Engineering, University of Southern California, Los Angeles, CA, USA. ⁷These authors contributed equally: Jacqueline F. Rivera, Haoyang Huang. ✉ e-mail: darnold@usc.edu

tracing from nonspecific cells, an adeno-associated virus (AAV1) and a genetically modified yellow fever virus (YFV), neither can mediate tracing from genetically determined cells^{14–16}.

Here, we introduce ATLAS (anterograde transsynaptic label based on antibody-like sensors), a rationally designed protein that mediates anterograde transsynaptic labeling from genetically determined cells. ATLAS can be expressed specifically in Cre-expressing neurons in transgenic animals and label neurons to which they project. Labeling is strictly anterograde, monosynaptic and activity-dependent *in vivo*. Furthermore, we provide direct evidence that transneuronal labeling mediated by ATLAS is exclusively transsynaptic. Finally, we show that components of ATLAS can be independently replaced, demonstrating that it is a versatile platform that can be upgraded or modified to perform specific tasks.

Results

Generating AF, a binder to the N terminus of GluA1

We used messenger RNA (mRNA) display, an *in vitro* selection procedure¹⁷, to identify binders to amino acids 1–394 of Rat GluA1 from a library of mRNA–protein fusions encoding the 10FNIII domain of human *FN1*, with 17 random residues engineered into the BC and FG loops^{18,19}. We expressed the selected fibronectin clones in COS7 cells with GluA1 fused to a hemagglutinin tag (GluA1-HA) and Stargazin-V5. Nonpermeabilized labeling of MYC showed that four fibronectin (Fn) clones labeled the surface of COS7 cells colabeled for HA (Extended Data Fig. 1). Following expression in dissociated cultures of cortical neurons, clone Fn9.3 gave the most robust labeling (Extended Data Fig. 1). We refer to this clone as AMPA.FingR (AF; FingR stands for fibronectin intrabody generated with mRNA display¹⁸).

We generated AF-HA protein and found that it bound specifically to a band colabeled with a GluA1 antibody on a western blot of neuronal lysate (Fig. 1a,b). To characterize AF further, we coexpressed a secreted version of it, ss-AF-YFP (ss refers to the GluA1 signal sequence), in dissociated cortical neurons with PSD-95.FingR-tagRFP, which labels postsynaptic sites¹⁸. We found that AF labeling partially overlapped with PSD-95.FingR-tagRFP, suggesting a perisynaptic localization (Fig. 1c and Extended Data Fig. 1). AF also colocalized with endogenous clathrin, consistent with localization to endocytic zones (Fig. 1d). We then tested whether AF-HA protein is endocytosed by adding it to the medium of cortical neurons in culture. We found that virtually all neurons displayed HA labeling (37 of 38, $n = 5$ independent cultures, Fig. 1e) within 1 h. Furthermore, the addition of 10 mg ml^{−1} chlorpromazine, a clathrin inhibitor, significantly reduced HA labeling (4.2 ± 0.8 versus 2.1 ± 0.5 , $P = 0.012$, $n = 5$ cultures, Mann–Whitney *U*-test, Fig. 1f), confirming that internalization was mediated by endocytosis. All values are expressed as mean \pm s.e.m.

Since AF binds to GluA1 receptors and is endocytosed postsynaptically, we reasoned that we could make a transsynaptic tracer if we targeted AF to synaptic vesicles by fusing it to the luminal domain of the presynaptic protein, synaptobrevin 2 (VAMP2) (ref. 20). We inserted a BACE1 (β -secretase) cleavage site (BACEcs)²¹ between AF and VAMP2 (to give VAMP2-BACEcs-AF), enabling endogenous BACE to cleave AF from VAMP2, leaving it free to exit the lumen of the synaptic vesicle on exocytosis. In addition, an ALFA-tag (At) was added to label VAMP2 (ref. 22). To test our strategy, we substituted super ecliptic pHluorin (SEP)²⁰ for AF and coexpressed the resulting plasmid (VAMP2-At-BACEcs-SEP, Fig. 1b) with PSD-95.FingR-tagRFP in cortical neurons in culture. The release from acidic synaptic vesicles into the neutral pH of the synaptic cleft is expected to cause a sudden increase in the fluorescence of SEP, allowing it to be visualized²⁰. Following overnight expression of VAMP2-At-BACEcs-SEP in neuronal cultures, we imaged SEP using widefield epifluorescence microscopy. We saw flashes of fluorescence lasting approximately 2–8 s (images taken at 1 Hz) appearing at points opposite postsynaptic sites (Fig. 1g). This result is consistent with VAMP2

delivering SEP to synaptic vesicles, BACE cleaving off SEP, and SEP being released into the synaptic cleft. We also fused AF to SEP and expressed the resulting protein (VAMP2-At-BACEcs-AF-SEP, Fig. 1b) in culture and observed flashes that were brighter and decayed with a longer time constant (6 ± 2 versus 405 ± 60 s, $n = 5$ independent cultures, Fig. 1h,i), a significant difference ($P < 0.0001$, *t*-test). This result is consistent with AF binding to the postsynaptic membrane following release and remaining until it is endocytosed. To further test whether AF-SEP is released from synaptic vesicles, we examined whether depolarization increases the number of release events. We imaged the same cultures before and after adding 100 mM KCl and counted the number of bright flashes corresponding to release events. We found a roughly 15-fold increase in release events with KCl (50 ± 6 versus 3 ± 1 for control, $P = 0.02$, *t*-test, $n = 5$ independent cultures; Fig. 1j–l). Together, these results are consistent with AF-SEP being released from synaptic vesicles, moving across the synaptic cleft, binding to the adjacent postsynaptic neuron perisynaptically and then being endocytosed.

Given that AF likely binds to the extracellular N-terminal domain of GluA1, we tested whether the expression of ss-AF-YFP affects synaptic transmission to hippocampal CA1 neurons. We found that in cells in hippocampal slices transfected with ss-AF-YFP using biolistics, the amplitudes of evoked excitatory postsynaptic currents (eEPSCs) of AMPA ($n = 10$, $P = 0.31$, *t*-test), NMDA receptors ($n = 8$, $P = 0.70$, *t*-test) and paired-pulse facilitation ($n = 6$, $P = 0.19$, *t*-test) were not significantly different from control cells, consistent with the expression of AF not affecting synaptic transmission (Fig. 1m–p). All pairs of recordings were made from distinct cultured slices and, thus, each is a biological replicate.

Transsynaptic tracing *in vitro* and *in vivo*

To generate a protein capable of mediating transsynaptic tracing, we replaced SEP with *Cre* in VAMP2-At-BACEcs-AF-SEP to give VAMP2-At-BACEcs-AF-*Cre* (ATLAS_{Cre}, Fig. 1b). Following expression of ATLAS_{Cre}, AF-*Cre* should be released into the synaptic cleft and then bind to AMPA receptors at the postsynaptic membrane. Subsequently, it needs to be endocytosed and carried to the nucleus to provide genetic access to the postsynaptic cell (Fig. 2a). To facilitate this final step, we added the DNA binding domain from CCR5 (refs. 18,23) to the ATLAS protein, as it contains a robust nuclear localization signal. To test our strategy, we transfected ATLAS_{Cre} into dissociated cultures infected with AAV encoding a floxed green fluorescent protein (GFP) reporter (AAV8-DIO-GFP). We observed cells with GFP and *Cre* that were not labeled with the starter cell marker, At, consistent with the transneuronal transport of *Cre* and recombination of the floxed allele, implying transport of *Cre* to the nucleus (Fig. 2b–e and Extended Data Fig. 2). Furthermore, At-labeled presynaptic structures were found to be overlapping or immediately adjacent to dendrites belonging to each of the GFP-labeled neurons (Extended Data Fig. 2). Thus, our results are consistent with ATLAS_{Cre} mediating transsynaptic tracing and providing genetic access to postsynaptic cells.

To test our strategy *in vivo*, we injected AAV8-ATLAS_{Cre} into the medial prefrontal cortex (mPFC) and AAV8-DIO-mCherry into the striatum (Str) of an adult mouse (Fig. 3a). After 1 week, we found At staining in mPFC and abundant mCherry staining in Str (Fig. 3b,c). In contrast, there was negligible mCherry staining in a control experiment without AAV8-ATLAS_{Cre} (Fig. 3d). Because the projection from mPFC to Str is strictly anterograde²⁴, this result is consistent with AAV8-ATLAS_{Cre} mediating the transsynaptic transport of *Cre* into the nucleus of the postsynaptic cell, causing mCherry labeling.

Tracing from genetically determined cells

To mediate genetically determined tracing, we generated AAV8-DIO-ATLAS_{FLP} (Fig. 1b), where expression of ATLAS is *Cre*-dependent and the payload is FLP (Flip recombinase). To test this

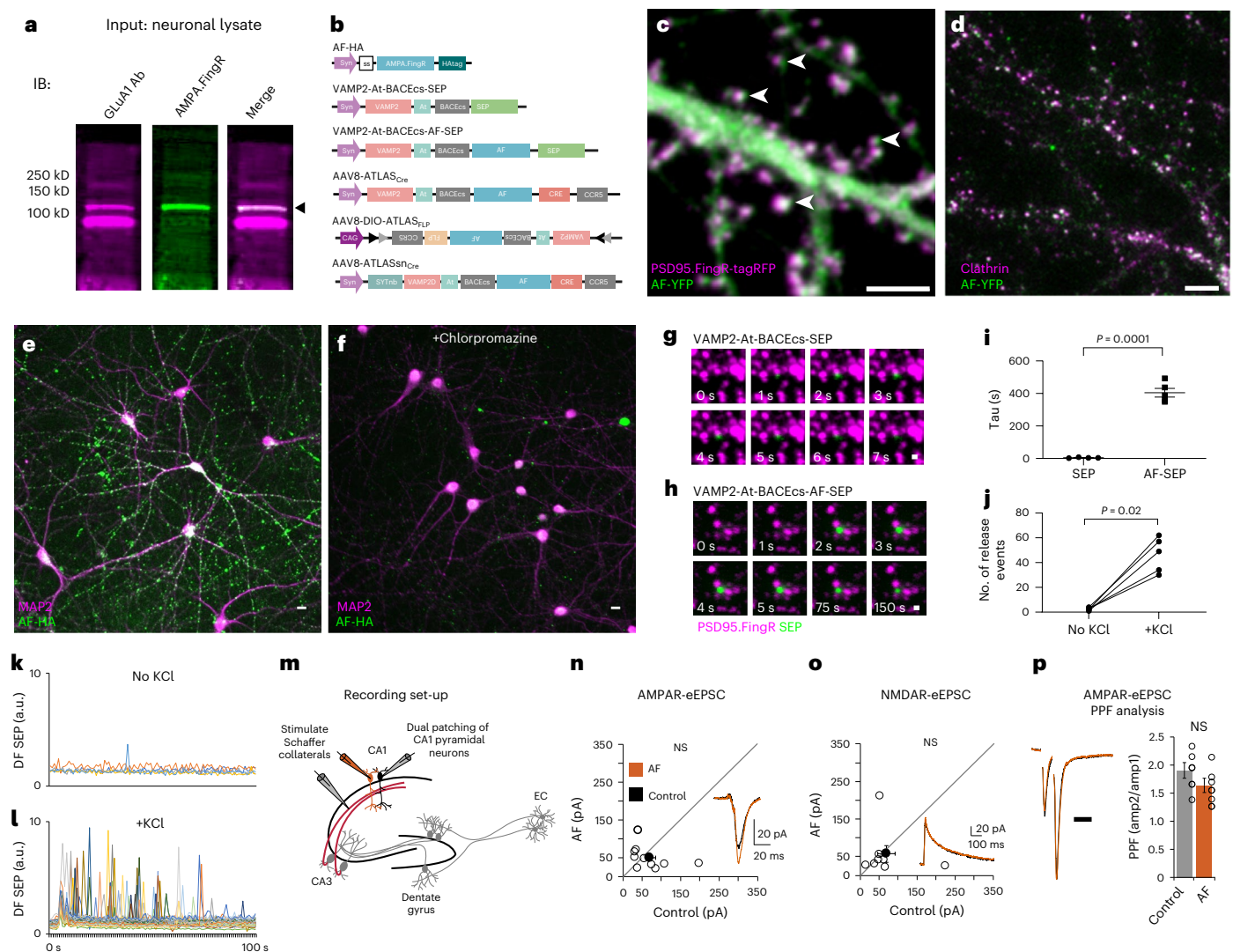


Fig. 1 | Mechanisms of release and uptake by ATLAS. **a**, Western blot of lysate from cortical cultures. IB, immunoblot. **b**, DNA constructs for testing of ATLAS. Arrows denote promoters. **c**, Live cultured neuron expressing ss-AF-YFP (green) and PSD-95.FingR-tagRFP (magenta). Scale bar, 5 μ m. **d**, Cultured neurons expressing ss-AF-YFP fixed and labeled for endogenous clathrin. Scale bar, 5 μ m. **e**, Neurons exposed to AF-HA protein (green) for 1 h and labeled for endogenous MAP2 (magenta). Scale bar 25 μ m. **f**, Same as **e**, but with the addition of 10 mg ml⁻¹ chlorpromazine to the culture medium. Scale bar, 25 μ m. **g**, Release of SEP from presynaptic sites in cultured cortical neurons expressing VAMP2-At-BACEs-SEP. PSD-95.FingR-tagRFP (magenta), SEP (green). Scale bar, 1 μ m. **h**, Same as **g**, but with VAMP2-At-BACEs-AF-SEP. Scale bar, 1 μ m. **i**, τ of VAMP2-At-BACEs-AF-SEP is significantly increased versus VAMP2-At-BACEs-SEP ($n = 5$, unpaired two-tailed t -test with Welch's correction). **j**, Adding 100 mM KCl to the culture medium causes a significant increase in the frequency of release events of VAMP2-At-BACEs-SEP ($n = 5$, paired two-tailed t -test). **k, l**, Graphs of the

differential (DF) of SEP fluorescence for VAMP2-At-BACEs-AF-SEP with control medium (**k**) versus with medium containing 100 mM KCl (**l**). Each spike denotes a single release event and does not reflect the duration of visible SEP fluorescence. **m**, Paired patch clamp recording of CA1 neurons in hippocampal slices (**n–p**). EC, entorhinal cortex. **n**, Biolistic transfection of CA1 pyramidal neurons with ss-AF-YFP did not significantly affect AMPAR-eEPSC amplitude ($n = 10$ pairs, $P = 0.31$, paired, two-tailed t -test). Scatterplots show eEPSC amplitudes for pairs of neighboring untransfected and transfected cells (open circles) with corresponding mean \pm s.e.m. (filled circles). Insets show representative current traces from control and transfected neurons with stimulation artifacts subtracted. **o**, Same as **n** for NMDAR-eEPSC amplitude ($n = 8$ pairs, $P = 0.70$, paired, two-tailed t -test). **p**, Right, bar graph shows mean \pm s.e.m. amplitude ratio of second AMPAR-eEPSC versus first ($n = 6$, $P = 0.19$, paired, two-tailed t -test). Left, representative current traces from control (gray) and transfected (orange) without stimulation artifacts. Scale bar, 50 ms. NS, not significant.

construct, we traced the projection from the primary visual cortex (V1) to the superior colliculus (SC), which is strictly anterograde²⁵. We coinjected Lenti-CamkII-Cre (a lentivirus expressing Cre specifically in excitatory neurons) and AAV8-DIO-ATLAS_{FLP} into V1 and AAV8-fDIO-mCherry into SC of wild-type mice. In addition to At staining in V1, we saw abundant staining for mCherry in SC (391 ± 37 cells, $n = 7$ samples from three mice, Fig. 3e–h and Supplementary Table 1) and a small number of faint cells on the control (35 ± 6 , $n = 6$ samples from three mice), which was subtracted from the previous count. All cell counts are expressed as the number of cells per 0.1 mm unless

otherwise specified to allow for comparisons. An advantage of this strategy is that lentivirus has no intrinsic retrograde or anterograde transneuronal transport that could cloud the interpretation of the results, unlike virtually every pseudotype of AAV¹⁵.

To test ATLAS tracing in transgenic Cre mouse lines, we examined the projection from the dorsal lateral geniculate nucleus (dLGN) to V1 in a VIPR2-Cre line expressing Cre in neurons in the dLGN²⁶. We injected AAV8-DIO-ATLAS_{FLP} into dLGN and AAV8-fDIO-mCherry into V1. Staining of At was found specifically in the dLGN, and mCherry staining in V1 (267 ± 54 cells, $n = 5$ samples from three mice) was dense

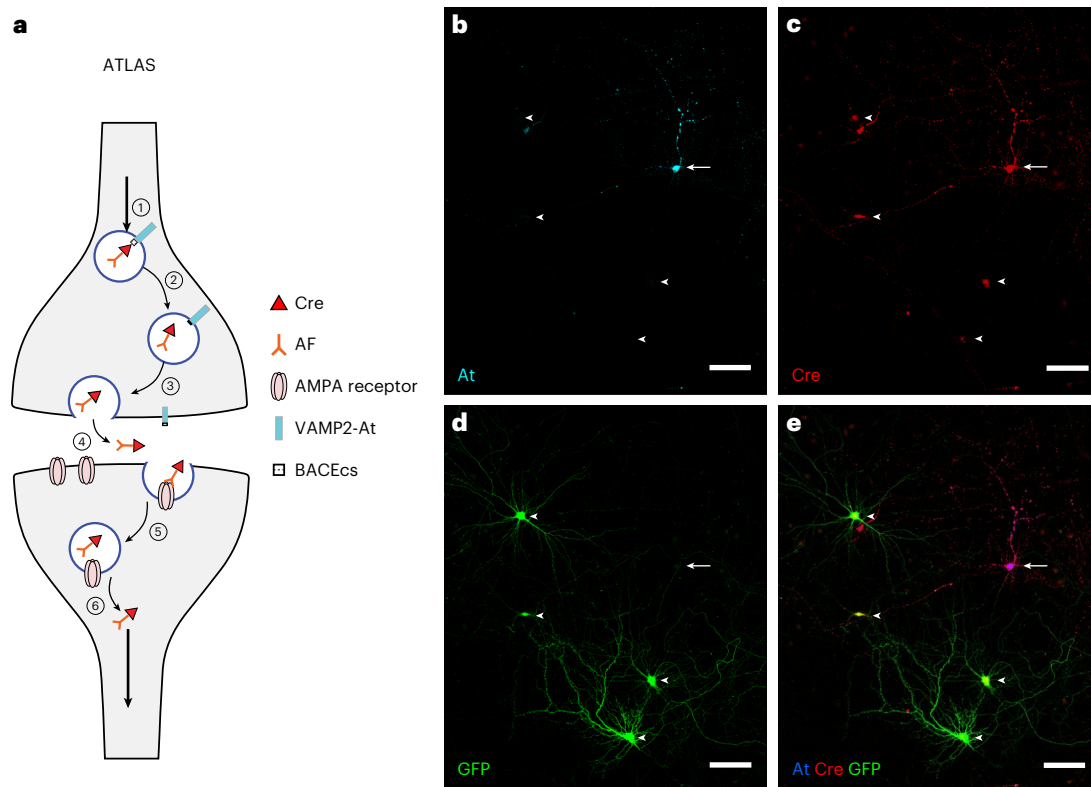


Fig. 2 | Schematic of ATLAS transsynaptic transport and testing in vitro. **a**, ATLAS_{Cre} protein (VAMP2-At-BACEs-AF-Cre) is expressed in a presynaptic starter cell and (1) targeted to synaptic vesicles by a VAMP2 domain. (2) A BACE cleavage site within the ATLAS protein is cleaved before release. (3) A peptide domain consisting of AF fused to Cre is released into the synaptic cleft and (4) subsequently binds to the extracellular domain of postsynaptic GluA1. (5) It is internalized through endocytosis and transported to the endosome. (6) AF-Cre moves to the nucleus, where Cre can catalyze the expression of a floxed reporter

gene. **b**, Cortical neuron in culture expressing ATLAS_{Cre} protein (arrow) following transfection, stained with anti-ALFA-tag (At) nanobody. Four other neurons shown (arrowheads) do not express At. **c**, Cre staining of the same neurons as in **b** including a neuron expressing ATLAS_{Cre} (arrow), and four not expressing ATLAS_{Cre} (arrowheads). **d**, GFP labeling of postsynaptic cells (arrowheads, green) following infection of AAV8-DIO-GFP. **e**, Combined labeling of At, GFP and Cre showing presynaptic (arrow) and postsynaptic neurons (arrowheads). Scale bars, 100 μ m.

in layer IV and less dense in layers II/III and V (Fig. 3i–l), consistent with known anatomy²⁷. These results are consistent with ATLAS tracing anterogradely from Cre-expressing neurons in wild-type and transgenic mice.

Increasing efficiency of transsynaptic labeling with BACE

To measure the efficiency of ATLAS tracing, we injected AAV8-ATLAS_{Cre} in mPFC and AAV8-DIO-mCherry in Str and counted the number of labeled cells as before after 1 week of incubation. Initially, we observed 144 ± 17 labeled cells ($n = 6$ samples from three mice). One possible inefficiency in our system is that there may be insufficient endogenous BACE in presynaptic cells to cleave all the AF-Cre from VAMP2. To test this hypothesis, we coexpressed exogenous BACE with ATLAS_{Cre} and measured the resulting efficiency. When we coinjected AAV8-BACE-HA and AAV8-ATLAS_{Cre} into mPFC in equal amounts, it did not significantly affect the number of postsynaptic cells labeled with mCherry (180 ± 20 cells, $n = 6$ samples from three mice, $P = 0.38$, Tukey's multiple comparisons, Extended Data Fig. 3). However, when we injected AAV8-BACE-HA and AAV8-ATLAS_{Cre} in a 5:1 ratio (viral particles), we saw a significant increase in the number of cells in Str labeled with mCherry, compared to both AAV8-ATLAS + BACE 1:1 ($P = 0.0027$) and AAV-ATLAS alone (286 ± 17 , $P = 0.0002$), $n = 6$ samples from three mice; Tukey's multiple comparisons test, Extended Data Fig. 3 and Supplementary Table 1). With this ratio of BACE to ATLAS, we saw approximately 10% of postsynaptic neurons labeled (Extended Data Fig. 3). Thus, when supplemented with exogenous BACE, ATLAS labels cells in the Str at a similar density to YFV¹⁴.

Labeling is transsynaptic

Given its design, it is likely that transneuronal labeling mediated by ATLAS occurs exclusively through synapses. To test this hypothesis in vivo, we asked whether transneuronal labeling could happen from inhibitory neurons. Since the uptake of ATLAS is mediated by GluA1 receptors, which are not found at inhibitory synapses, if we expressed ATLAS in inhibitory neurons, any transneuronal labeling would have to be nonsynaptic (Fig. 4a). Accordingly, we injected AAV8-DIO-ATLAS_{FLP} and AAV8-fDIO-mCherry into V1 of an SST-Cre mouse, where somatostatin-positive inhibitory interneurons express Cre²⁸. When we examined labeling in the cortex after 2 weeks, we saw 483 cells labeled with mCherry and, of those, only 20 cells were not colabeled with At (Fig. 4b–d and Supplementary Table 1, $n = 3$ mice). This labeling rate was less than the background rate measured over an equivalent number of sections for control experiments where only AAV8-fDIO-mCherry was injected into V1 (100 cells, $n = 3$ mice), consistent with no transneuronal labeling above background. This result leads us to conclude that ATLAS labels postsynaptic neurons exclusively through the transsynaptic transfer of proteins.

ATLAS tracing does not block synaptic transmission

To test whether ATLAS disrupts synaptic transmission, we coinjected AAV8-ATLAS_{SsnCre} (Fig. 1b), AAV8-BACE-HA and AAV8-DIO-Channelrhodopsin 2 (ChR2)-GFP into the mPFC and AAV8-DIO-mCherry in the Str of wild-type mice. Since we found that ATLAS labels ~10% of target neurons in this circuit (Extended Data Fig. 3), we reasoned that it should be possible to find both labeled and nonlabeled cells that

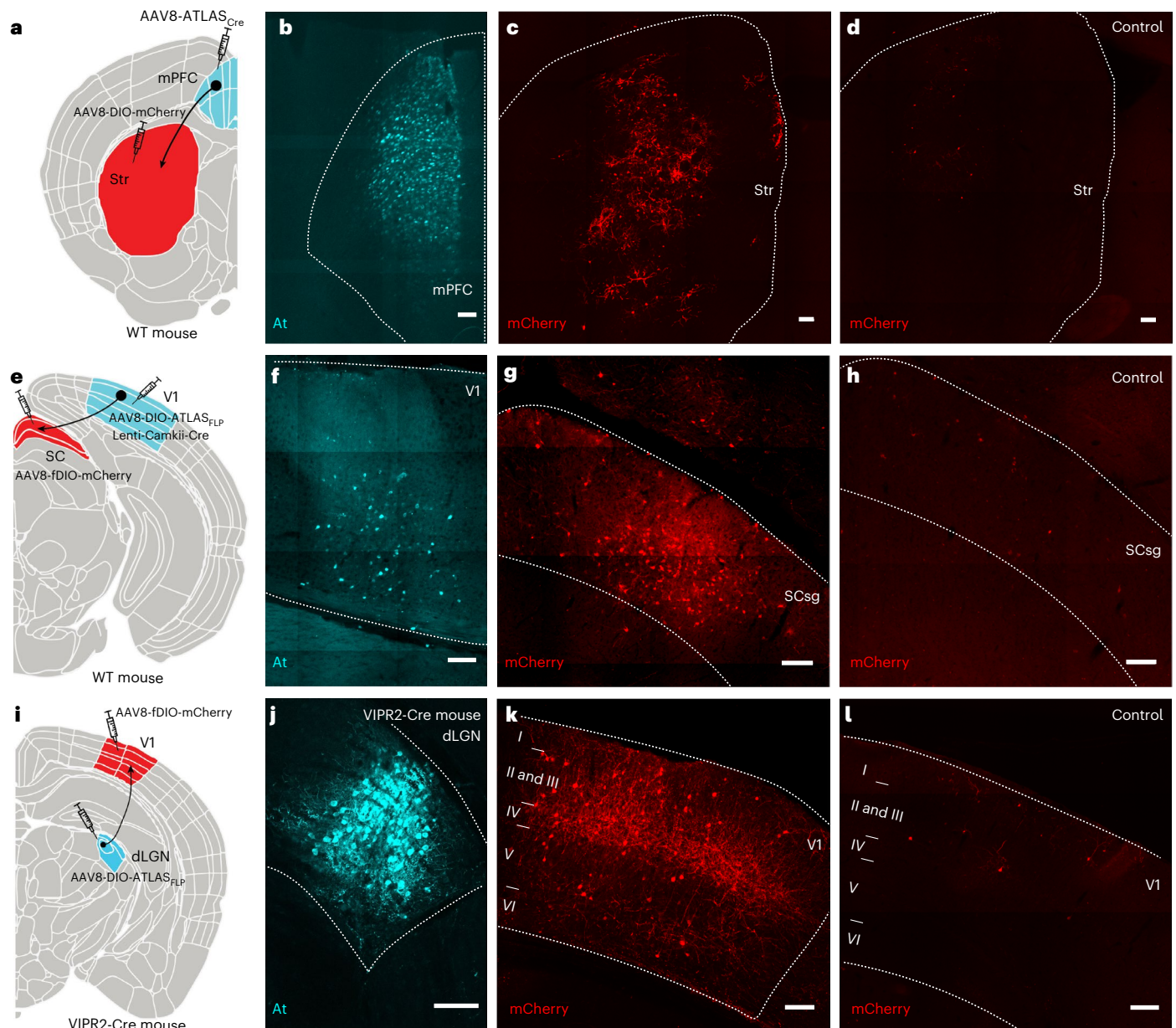


Fig. 3 | ATLAS mediates transsynaptic tracing in vivo. **a**, Schematic depicting injections of AAV8-ATLAS_{Cre} into the mPFC (cyan) and AAV8-DIO-mCherry into the Str (red) to trace the unidirectional projection from the mPFC to Str. **b**, ALFA-tag (At) staining of ATLAS_{Cre} in presynaptic cells in mPFC in a wild-type (WT) mouse. **c**, mCherry staining of postsynaptic cells in Str in the same brain as **b**. **d**, Control brain injected only with AAV8-DIO-mCherry in Str. **e**, Schematic depicting injections of AAV8-DIO-ATLAS_{FLP} and Lenti-CamkII-Cre into the primary visual cortex (V1, cyan) and AAV8-fDIO-mCherry into the SC (red) to

trace the unidirectional projection from V1 to SC. **f**, At staining of ATLAS_{FLP} in presynaptic cells in V1 in a wild-type mouse. **g**, mCherry staining of postsynaptic cells in SC in the same brain as **f**. **h**, Control brain injected only with AAV8-fDIO-mCherry in SC. **i**, Schematic depicting injections of AAV8-DIO-ATLAS_{FLP} into the dLGN (cyan) and AAV8-fDIO-mCherry into V1 (red) to trace the projection from dLGN to V1 in a VIPR2-Cre mouse. **j**, At staining of ATLAS_{FLP} in presynaptic cells in dLGN. **k**, mCherry staining of postsynaptic cells in the V1 in the same brain as **j**. **l**, Control brain injected with only AAV8-fDIO-mCherry in V1. Scale bars, 100 μ m.

are synaptically connected to ChR2-expressing neurons to compare whether ATLAS labeling affects the cell's physiological properties. Four weeks after the virus injection, we cut coronal slices of Str approximately 350 μ m thick and incubated them in artificial cerebral spinal fluid for in vitro slice recording. Whole-cell patch clamp recording was performed to measure 470-nm optically evoked EPSC (eEPSC) from striatal cells (Extended Data Fig. 4). To evaluate the potential effect of ATLAS tracing on synaptic transmission, we compared the striatal cells with and without mCherry expression. Robust evoked EPSCs were recorded in mCherry-expressing cells with an onset latency of <5 ms following the light flash in eight out of eight cells (from three mice), indicating that the presynaptic ChR2-expressing cells were

synaptically connected with mCherry-labeled cells (Extended Data Fig. 4). Furthermore, when labeled postsynaptic cells were recorded from, the amplitude of ChR2-evoked EPSCs exhibited a nonsignificant increase compared with those of unlabeled cells (Extended Data Fig. 4, $n = 8$ labeled cells, $n = 7$ unlabeled cells from three mice for both, $P = 0.28$, t -test). Thus, ATLAS did not block synaptic transmission. In addition, there were no significant changes in onset latency ($P = 0.22$, t -test) and time constant ($P = 0.78$, t -test, Extended Data Fig. 4). This result is consistent with transsynaptic labeling with ATLAS not causing detectable toxicity. Moreover, we verified that evoked currents are monosynaptic through the sequential application of Tetrodotoxin, which blocks action potentials and polysynaptic transmission, and

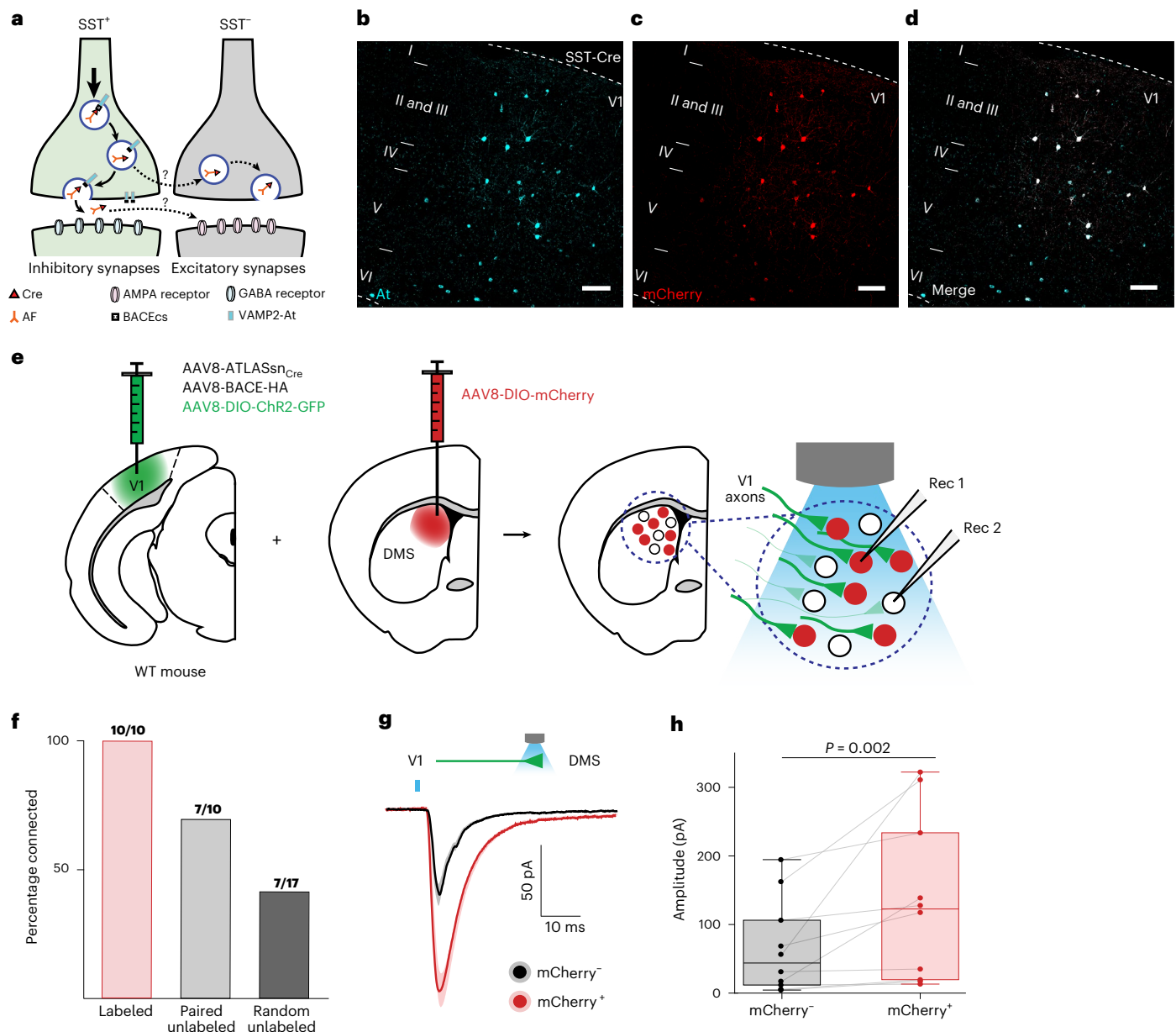


Fig. 4 | ATLAS does not mediate nonsynaptic transneuronal labeling and transsynaptic labeling is specific. **a**, Schematic of possible nonsynaptic pathways for transneuronal labeling from an SST⁺ neuron. **b**, SST-Cre mouse with AAV8-DIO-ATLAS_{FLP} and AAV8-DIO-mCherry co-injected into V1. Labeling of inhibitory presynaptic neurons with At. This experiment was performed in two mice and bilaterally in one of the mice, for a total of three biological replicates. **c**, mCherry-labeled neurons from the same brain as in **a**. **d**, Merged mCherry and At labeling shows that all neurons labeled with mCherry are also labeled with At. **e**, Schematic of configuration for whole-cell patch clamp recording from random pairs of mCherry- or tdTomato-labeled and unlabeled striatal spiny projection neurons following ATLAS-mediated tracing from V1 cortex. EPSCs were generated as a result of optical activation of inputs from the V1.

cortex. **f**, Percentage of cells of different types with nonzero amplitude EPSCs following exposure to blue light: 100% of mCherry-labeled neurons, 70% of paired unlabeled neurons, ~40% of random, unlabeled neurons. **g**, Comparison of average EPSC trace from all optically evoked EPSCs from mCherry⁺ and paired mCherry⁻ striatal spiny projection neurons. **h**, EPSC amplitudes of mCherry⁺ and mCherry⁻ neurons (n = 10). In ten out of ten pairs, the amplitude of the EPSC recorded from mCherry-labeled neuron is larger than that of the EPSC recorded from the corresponding unlabeled neuron (Wilcoxon signed-rank test). Box plot, the central mark indicates the median, and the bottom and top edges of the box indicate the 25th and 75th percentiles, respectively. The whiskers extend to the most extreme data points not considered outliers. Scale bar, 100 μm.

4-aminopyridine, which blocks K⁺ channels and facilitates direct activation of presynaptic terminals.

Electrophysiology confirms specificity of ATLAS tracing

To test for the specificity of ATLAS tracing, we measured optogenetically evoked currents in the circuit from the primary visual cortex to the Str²⁹. We coinjected AAV8-ATLAS_{SsnCre} (Fig. 1b) and AAV8-BACE-HA in V1, and AAV8-DIO-mCherry/tdTomato in the dorsomedial Str (DMS).

Two weeks later, we injected AAV8-DIO-ChR2-GFP in the same area in V1 as the first injection to manipulate ATLAS-labeled presynaptic inputs while minimizing expression competition between ATLAS and ChR2. Histology 2 weeks after the second injection revealed efficient expression of At, HA, ChR2 in V1 and Cre-dependent mCherry/tdTomato in DMS, consistent with the projection pattern of DMS-projecting V1 neurons (Extended Data Fig. 4). To compare V1 innervation between ATLAS-labeled versus unlabeled postsynaptic neurons, we measured

optically evoked EPSCs (oEPSCs) following a 2-ms flash of 473-nm blue light in acute brain slices prepared from mice injected with virus 4 weeks earlier (Fig. 4e). We performed sequential, paired whole-cell recordings where we measured oEPSCs of an ATLAS-labeled (mCherry/tdTomato⁺) and an unlabeled (mCherry/tdTomato⁻) neuron in the same field of view (100 × 100 μm; Fig. 4e–h). Ten pairs of cells (from four mice) were recorded, in which ten out of ten labeled cells carried a current, compared with seven out of ten unlabeled cells (Fig. 4f). To assess the baseline connection probability of the V1-DMS circuit, we randomly patched onto DMS neurons in striatal areas where we saw prominent fiber labeling with GFP. Of the 17 random cells we patched ($n = 3$ mice), 41% of cells were connected (7 out of 17, Fig. 4f). oEPSCs recorded from labeled cells were significantly larger in amplitude and total charge compared with those of paired unlabeled cells (amplitude -134 ± 38 versus -66 ± 21 pA, $P = 0.0020$, Wilcoxon signed-rank test, total charge -0.121 ± 0.03 versus -0.038 ± 0.01 pC, $P = 0.0020$, Wilcoxon signed-rank test, $n = 10$ mice, plotted as absolute values in Fig. 4g,h). Furthermore, in ten out of ten pairs, the current recorded from the labeled cell had a larger amplitude than that from the unlabeled cell (Fig. 4h). Together, these results indicate that when ATLAS_{Cre} and a Cre-dependent reporter are simultaneously expressed in different brain regions, cells exhibiting Cre-dependent labeling are likely to receive synaptic inputs from cells expressing ATLAS_{Cre}. Furthermore, they demonstrate that cells with stronger synaptic connections are more likely to be labeled by ATLAS.

ATLAS is exclusively anterograde and monosynaptic

A limitation of many virally based anterograde transneuronal labeling methods is that they also mediate labeling in the retrograde direction^{14,15}. To determine whether ATLAS mediates retrograde labeling in vivo, we injected AAV8-DIO-ATLAS_{FLP} and Lenti-hsyn-Cre into Str and AAV8-fDIO-mCherry into mPFC (Fig. 5a). Because the mPFC to Str projection is unidirectional and lentivirus does not spread retrogradely, any labeling in mPFC would be due to retrograde transneuronal labeling mediated by ATLAS. However, despite abundant At labeling in Str, indicating that ATLAS was expressed at a high level, we found no labeling above background in mPFC (20 ± 4 cells for experiment, $n = 6$ samples from three mice, versus 45 ± 14 for control, $n = 6$ samples from three mice, $P = 0.11$, t -test, Fig. 5b–e and Supplementary Table 1). These data are consistent with ATLAS not mediating retrograde labeling.

To test whether ATLAS can mediate transsynaptic labeling that is monosynaptic, a critical property for transsynaptic tracing results to be interpretable, we tried tracing the polysynaptic pathway from V1 to SC to the parabrachial nucleus (PBG)¹⁴. We injected AAV8-ATLAS_{Cre} into V1 and AAV8-DIO-mCherry into SC and PBG (Fig. 5f). We found AT labeling in V1 and abundant transsynaptic mCherry labeling in SC (Fig. 5g,h) but no staining significantly above background in PBG (3 ± 1 cells for experiment, $n = 8$ samples from three mice, versus 19 ± 3 for control, $n = 6$ samples from three mice, $P = 0.35$, one-way analysis of variance (ANOVA) (Tukey's test, Fig. 5i,n). Furthermore, when we injected AAV8-ATLAS_{Cre} into SC, we saw abundant labeling in PBG (181 ± 30 cells, $n = 3$ samples from three mice) that was significantly above both background and labeling from V1 to PBG ($P < 0.0001$ for both, one-way ANOVA, Tukey's multiple comparisons, Fig. 5j–n), demonstrating that ATLAS is capable of tracing the SC to PBG pathway. Thus, transsynaptic labeling mediated by ATLAS is exclusively anterograde and monosynaptic.

Activity dependence of ATLAS

Because ATLAS mediates transsynaptic labeling by releasing AF-recombinase from synaptic vesicles, transsynaptic labeling is likely activity-dependent. To test for activity dependence of transsynaptic labeling in vivo, we injected AAV8-ATLAS_{Cre} + AAV8-hHM3Dq-mCherry, an excitatory DREADD³⁰, into mPFC and AAV8-DIO-GFP into Str (Extended Data Fig. 5) in two mice. We then injected one mouse daily

with clozapine N-oxide (CNO) intraperitoneally but not the other. After 1 week, we perfused the mice and performed immunocytochemistry. We found abundant c-FOS labeling in the mPFC of the CNO⁺ mouse, which overlapped with At labeling (Extended Data Fig. 5 and Supplementary Table 1). In contrast, there was negligible c-FOS labeling in the mPFC of the CNO⁻ mouse (Extended Data Fig. 5 and Supplementary Table 1). In addition, GFP labeling appeared to increase in terms of total fluorescence and number of labeled cells in the CNO⁺ mouse (Extended Data Fig. 5). We then pooled these data with those from similar experiments using AAV8-ATLAS_{Cre} and found that CNO⁺ mice had significantly higher postsynaptic GFP labeling in the Str versus CNO⁻ mice both in terms of the number of cells labeled (88 ± 12 versus 52 ± 7 , $n = 5$ mice, $P = 0.0357$, t -test, Extended Data Fig. 5) and total fluorescence (38 ± 4 versus 19 ± 2 a.u., $P = 0.0025$, t -test, Extended Data Fig. 5). In contrast, the number of presynaptic At stained cells was not significantly different between CNO⁺ and CNO⁻ mice ($1,200 \pm 100$ versus $1,200 \pm 100$, $P = 0.7492$, t -test, Extended Data Fig. 5). Thus, our results indicate that the efficiency of transsynaptic labeling was significantly higher in CNO⁺ mice versus CNO⁻ mice, consistent with ATLAS mediating activity-dependent transsynaptic labeling.

An alternate synaptic vesicle targeting domain

ATLAS is composed of multiple independent components, each of which can, in principle, be modified or upgraded to improve efficiency or alter function. We took advantage of this property to optimize the VAMP2 component of ATLAS, which is responsible for presynaptic targeting. Although VAMP2 is widely used as a presynaptic marker, it can produce toxicity when expressed at a high level. Indeed, we saw evidence of toxicity when ATLAS was expressed in the mPFC for 2 and 4 weeks (Extended Data Fig. 6). Accordingly, we exchanged the cytoplasmic domain of VAMP2 for a nanobody against Synaptotagmin 1 (SYTnb)³¹ to give SYTnb-VAMP2Δ-At-BACEcs-AF-Cre (ATLAS_{Cre}, Figs. 1b and 6a), where VAMP2Δ consists of the luminal and transmembrane domains of VAMP2. When we expressed ATLAS_{Cre} in the mPFC for 2 or 4 weeks, we saw no evidence of toxicity (Extended Data Fig. 6). To test ATLAS_{Cre}, we transduced it into dissociated cultures of cortical neurons while infecting them with AAV8-DIO-mCherry. We saw abundant cells labeled with mCherry but not with At, indicating they were labeled transsynaptically (Fig. 6b). A closeup image of such a postsynaptic cell revealed At labeling opposite its dendritic spines, consistent with presynaptic labeling (Fig. 6b, inset).

To test AAV8-ATLAS_{Cre} in vivo, we injected it and AAV8-BACE-HA into the mPFC and AAV8-DIO-mCherry into the Str. After 2 weeks of incubation, we saw expression of At in the mPFC and abundant mCherry labeling in Str (Fig. 6c,d and Extended Data Fig. 7). The dorsal region of postsynaptic mCherry labeling colocalized almost perfectly with At labeling representing presynaptic termini (Fig. 6d and Extended Data Fig. 7), consistent with ATLAS_{Cre} mediating transsynaptic labeling. To further test ATLAS_{Cre} in vivo, we coinjected AAV8-ATLAS_{Cre} and AAV8-BACE-GFP in M1 cortex and AAV8-DIO-mCherry in the Str and thalamus (Thal, Fig. 6e). After 2 weeks of incubation, staining of GFP and mCherry revealed labeled presynaptic cells in M1 (Fig. 6f) and postsynaptic cells in Str (Fig. 6g) and Thal (Fig. 6h). Overlap of GFP and mCherry labeling in Str and Thal (Extended Data Fig. 7) is consistent with transsynaptic labeling. Furthermore, minimal background was observed in the Str when AAV8-DIO-mCherry alone was injected (Extended Data Fig. 7).

Labeling of cortical to subcortical circuits

To further test ATLAS_{Cre}, we used it to trace three additional pathways: from the auditory cortex (A1) to the inferior colliculus, the mPFC to the claustrum and the entorhinal cortex to the hippocampus, respectively. In each case, we injected AAV8-ATLAS_{Cre} and AAV8-BACE-HA into the presynaptic area and AAV8-DIO-GFP into the corresponding postsynaptic area. After 2 weeks, we stained presynaptic cells for At

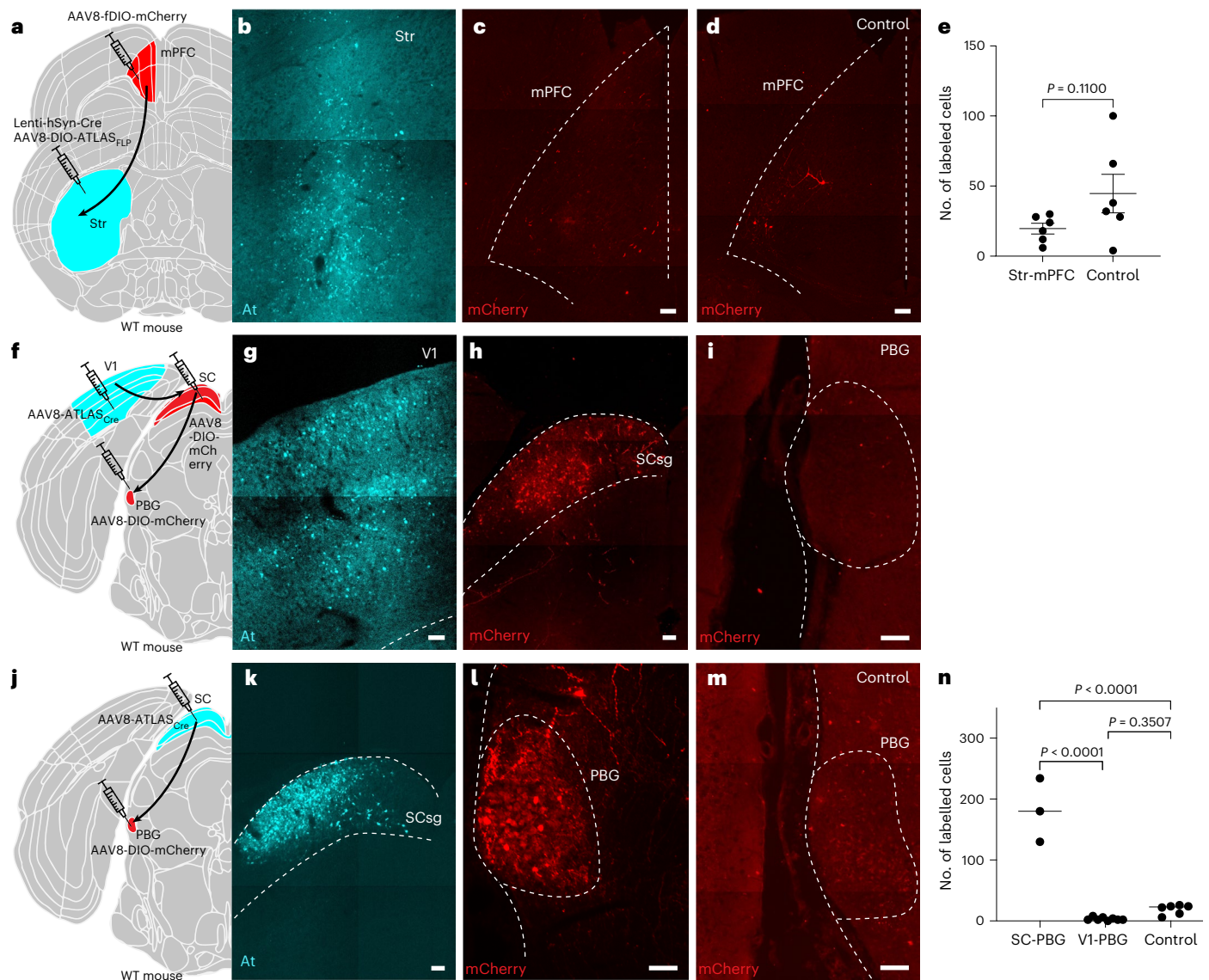


Fig. 5 | Transsynaptic labeling by ATLAS is exclusively anterograde and monosynaptic. **a**, Schematic of the projection from mPFC to Str showing injections of AAV8-DIO-ATLAS_{FLP} and Lenti-hsyn-Cre (Str, cyan), and AAV8-fDIO-mCherry (mPFC, red). **b**, At labeling of cells in Str. **c**, mCherry labeling of cells in mPFC in the same brain as **b**. **d**, mCherry labeling of cells in mPFC in a control mouse brain with an injection of AAV8-fDIO-mCherry into the mPFC only. **e**, Number of labeled postsynaptic cells following Str-mPFC labeling is not significantly different from control mPFC (t -test, $n = 6$, Str-mPFC; $n = 6$, control). **f**, Schematic of the disynaptic pathway from V1 to SC to PBG showing injection of ATLAS_{Cre} (V1) and AAV8-DIO-mCherry (SC and PBG) for **f-h**. **g**, At labeling of

presynaptic cells in V1. **h**, mCherry labeling of postsynaptic cells in the superficial gray layer of the SC (SCsg) from the same brain as **g**. **i**, mCherry labeling in PBG from the same brain as **f** and **g**. **j**, Schematic of projection from SCsg to PBG showing injections of ATLAS_{Cre} (SCsg) and AAV8-DIO-mCherry (PBG). **k**, At labeling of presynaptic cells in SCsg. **l**, mCherry labeling of postsynaptic cells in PBG from the same brain as **k**. **m**, mCherry labeling in PBG following injection of AAV8-DIO-mCherry into PBG only in a control mouse brain. **n**, Number of labeled postsynaptic cells following SC-PBG labeling is significantly more than following V1-PBG labeling (one-way ANOVA). Scale bars, 100 μ m.

and postsynaptic cells for GFP. In each experiment, we found cells with At and GFP labeling, consistent with efficient transsynaptic labeling (inferior colliculus, 173 ± 13 cells, $n = 8$ samples from three mice; claustrum, 71 ± 14 cells, $n = 7$ samples from three mice; hippocampus, 132 ± 30 cells, $n = 4$ samples from two mice, Extended Data Fig. 8 and Supplementary Table 1). Thus, ATLAS is capable of tracing multiple different pathways.

In addition, to understand the time course over which transsynaptic labeling happens, we coexpressed AAV8-ATLAS_{SnCre} and AAV8-BACE-HA in the mPFC and AAV8-DIO-GFP in the Str and waited 4, 7, 14 and 21 days ($n = 8$ samples from four mice in each case) before perfusing animals and staining for presynaptic and postsynaptic labels. After 4 days, we found faint labeling of presynaptic cells with

At, although labeled cells were relatively abundant (534 ± 114 cells, Extended Data Fig. 9). In contrast, GFP-labeled postsynaptic cells were very sparse at this time point (2 ± 1 cells), and total GFP labeling was minimal (3 ± 1 a.u.). After 7 days, the number of presynaptic cells labeled with At increased ($1,150 \pm 300$, Extended Data Fig. 9), but not significantly ($P = 0.3279$, one-way ANOVA). However, both the number of labeled postsynaptic cells (52 ± 7 cells) and the total GFP label (35 ± 3 a.u.) were significantly higher ($P < 0.0001$, ANOVA; Extended Data Fig. 9). Thus, postsynaptically labeled cells become visible between 4 and 7 days postinjection. After 14 and 21 days, the number of labeled presynaptic cells ($1,270 \pm 260$ and $1,070 \pm 270$ cells) was not significantly different from 7 days ($P = 0.9874$, $P = 0.9943$, ANOVA; Extended Data Fig. 9). The number of postsynaptic cells

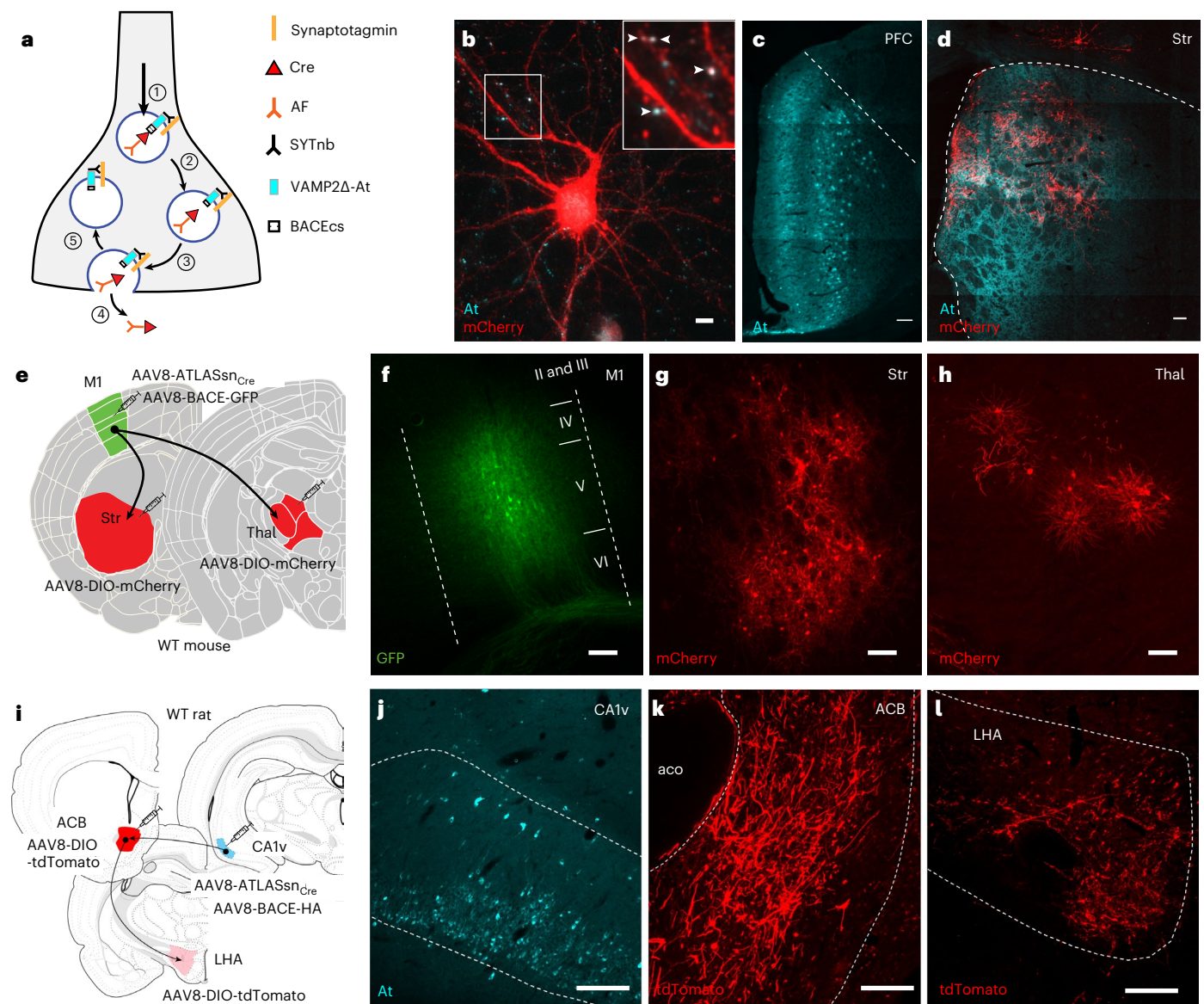


Fig. 6 | Transsynaptic tracing with ATLASsn. **a**, Schematic of ATLASsn. (1) Synaptotagmin nanobody (SYTnb) fused to the transmembrane domain of VAMP2 (VAMP2Δ) targets ATLAS to synaptic vesicles. (2) AF-Cre is cleaved from VAMP2Δ. (3) The synaptic vesicle fuses with the plasma membrane at the presynaptic terminal. (4) AF-Cre is released into the synaptic cleft. (5) SYTnb-VAMP2Δ-At is recycled back into the terminal, labeling the presynaptic site. **b**, ATLAS tracing in dissociated cortical culture transfected with AAV8-ATLASsnCre (labeled with At, cyan) and AAV8-BACE-HA and infected with AAV8-DIO-mCherry. Scale bar, 10 μm. **c**, mPFC of the mouse injected with AAV8-ATLASsnCre (cyan) and incubated for 2 weeks. This experiment was performed in three mice. **d**, Str of the same mouse as in **c**, injected with AAV8-DIO-mCherry (red). **e**, Schematic showing projections from the M1 to Str and thalamus (Thal).

This experiment was performed in three mice. **f**, M1 of a mouse coinjected with AAV8-BACE-GFP (green) and AAV8-ATLASsnCre. **g**, Str of the same mouse as in **f** injected with AAV8-DIO-mCherry showing mCherry-labeled neurons (red). This experiment was performed in three mice. **h**, Thalamus of the same mouse as in **f** and **g** injected with AAV8-DIO-mCherry showing mCherry-labeled neurons (red). **i**, Schematic showing pathway from the ventral CA1 to the nucleus accumbens (ACB) and then to the LHA in the rat. This experiment was performed in three rats. **j**, Ventral CA1 region of a rat injected with AAV8-ATLASsnCre showing cell labeled with At (cyan). **k**, ACB of the same rat as in **j** injected with AAV8-DIO-tdTomato, showing tdTomato-labeled neurons (red): aco refers to the anterior commissure. **l**, LHA of the same rat as in **j** and **k** showing nerve terminals labeled with tdTomato (red). Scale bars 100 μm in **c,d,f,g,h**, 500 μm in **j**; 200 μm in **k,l**.

labeled with GFP at 14 days (63 ± 5 cells) was not significantly different from the number at 7 days ($P = 0.4514$, ANOVA; Extended Data Fig. 9). However, the cell number at 21 days (86 ± 5 cells) was significantly higher than at 14 days ($P = 0.0116$, ANOVA). The labeling intensity increased significantly at 14 and 21 days versus 7 days (65 ± 2 and 82 ± 6 a.u., $P < 0.0001$, ANOVA; Extended Data Fig. 9). Thus, ATLAS transsynaptic labeling increases notably in the first 7 days and at a slower rate thereafter in terms of cell number, but increases in a relatively linear manner in total intensity. In contrast, labeling of presynaptic cells is constant after the first week.

ATLAS mediates transsynaptic labeling in the rat

It is highly desirable for transsynaptic labeling techniques to work in systems other than the mouse. Accordingly, we tested whether ATLAS would work in the rat by injecting AAV8-ATLASsnCre and AAV8-BACE-HA into the CA1 region of the ventral hippocampus and AAV8-DIO-tdTomato into the nucleus accumbens (ACB, Fig. 6i), to which the CA1 neurons project. We observed At staining in CA1 (Fig. 6j) and abundant tdTomato-labeled cells in ACB (115 ± 11 , $n = 3$ rats, Fig. 6k), consistent with transsynaptic labeling. Finally, tdTomato labeling of axons within the lateral hypothalamic area (LHA) (Fig. 6l), which

receives axonal projections from ACB³², confirms the postsynaptic labeling of neurons within ACB.

Discussion

ATLAS is a rationally designed protein that mediates transsynaptic tracing from genetically determined neurons via a precisely defined mechanism. In contrast, viruses such as rabies, YFV, AAVs and the protein used in the nonviral method Trans-Seq have modes of egress from starter cells and entry into recipient cells that remain mysterious^{10,14,15,33}. In addition, AAV1, YFV, vesicular stomatitis virus (VSV) and herpes simplex virus-1 (HSV1) undergo a measurable component of retrograde transport in addition to anterograde and have not been shown to mediate tracing that is exclusively transsynaptic^{14–16,34,35}.

Because ATLAS protein does not have an intrinsic amplification mechanism like rabies and similar viruses⁹, tracing using ATLAS requires the expression of a recombinase-dependent reporter in the postsynaptic cell. While this could be interpreted as a drawback, it is also a benefit because amplification that occurs in rabies or VSV infection is associated with toxicity^{36,37}. In the case of tracing using AAV1, which also requires amplification, a transgenic mouse with a floxed reporter transgene can be used instead of postsynaptic injections^{15,16}. Efficient and consistent transsynaptic labeling occurred in some but not all cases when we expressed ATLAS_{Cre} in the ai75 floxed reporter mice³⁸. Thus, broad regions containing postsynaptic target areas must be identified a priori and injected with a floxed reporter, which is not required for many virus-based transneuronal labeling techniques. However, this should not be a difficult problem to surmount as regions postsynaptic to specific cell types are easily identified by exogenously expressing a presynaptic marker such as VAMP2 (ref. 39).

Our finding that 100% of postsynaptic striatal cells labeled following expression of ATLAS in V1 were synaptically connected to cells expressing ChR2-GFP, which was coinjected with ATLAS, indicates that postsynaptic cells with Cre-dependent labeling are likely to be synaptically connected with presynaptic starter cells in which ATLAS_{Cre} is expressed. Also, 70% of neurons not labeled with ATLAS but immediately adjacent to labeled cells were found to be connected to presynaptic cells expressing ChR2-GFP. This result could be due to many factors, including the fact that transsynaptic labeling with ATLAS is not 100% efficient. In addition, Cre-dependent expression of ChR2-GFP could occur in neurons in V1 that are connected with starter cells through local connections, leading to more widespread expression of ChR2-GFP than of ATLAS. In contrast to paired unlabeled neurons, ~40% of random unlabeled cells chosen near labeled presynaptic terminals from V1 were found to be connected to those terminals. These data are consistent with postsynaptic neurons labeled with ATLAS being connected to labeled presynaptic neurons at a rate considerably higher than chance.

Because ATLAS is a protein, it can be evolved to change its properties and improve performance similar to GCaMP⁴⁰ or GRAB sensors⁴¹. For instance, ATLAS, as described in this paper, works only for anterograde tracing from excitatory neurons. However, AF can, in principle, be replaced by a recombinant binder to a neurotransmitter receptor, such as a GABA (γ -aminobutyric acid) or acetylcholine receptor, or even to a receptor for a neuromodulator, such as dopamine or serotonin. The resulting modified ATLAS could be used for tracing virtually any neuronal circuit mediated by the corresponding neurotransmitter–receptor combination. Also, because of its activity dependence, ATLAS could be used to mark circuits that respond to specific stimuli, especially if ATLAS tracing could be gated to occur during a particular time interval. Finally, it may be possible to modify ATLAS to label circuit changes during events such as memory formation⁴² or specific developmental processes such as synaptic pruning⁴³.

Online content

Any methods, additional references, Nature Portfolio reporting summaries, source data, extended data, supplementary information,

acknowledgements, peer review information; details of author contributions and competing interests; and statements of data and code availability are available at <https://doi.org/10.1038/s41592-025-02670-x>.

References

- Weber, F. & Dan, Y. Circuit-based interrogation of sleep control. *Nature* **538**, 51–59 (2016).
- Zhao, Q. et al. A multidimensional coding architecture of the vagal interoceptive system. *Nature* **603**, 878–884 (2022).
- Condylis, C. et al. Dense functional and molecular readout of a circuit hub in sensory cortex. *Science* **375**, eabl5981 (2022).
- Bayless, D. W. et al. A neural circuit for male sexual behavior and reward. *Cell* **186**, 3862–3881 e3828 (2023).
- Jarvie, B. C. & Knight, Z. A. Breaking down a gut-to-brain circuit that prevents malabsorption. *Cell* **185**, 2393–2395 (2022).
- Kohl, J. et al. Functional circuit architecture underlying parental behaviour. *Nature* **556**, 326–331 (2018).
- Network, B. I. C. C. A multimodal cell census and atlas of the mammalian primary motor cortex. *Nature* **598**, 86–102 (2021).
- van der Want, J. J., Klooster, J., Cardozo, B. N., de Weerd, H. & Liem, R. S. Tract-tracing in the nervous system of vertebrates using horseradish peroxidase and its conjugates: tracers, chromogens and stabilization for light and electron microscopy. *Brain Res. Protoc.* **1**, 269–279 (1997).
- Callaway, E. M. & Luo, L. Monosynaptic circuit tracing with glycoprotein-deleted rabies viruses. *J. Neurosci.* **35**, 8979–8985 (2015).
- Wickersham, I. R., Finke, S., Conzelmann, K. K. & Callaway, E. M. Retrograde neuronal tracing with a deletion-mutant rabies virus. *Nat. Methods* **4**, 47–49 (2007).
- Weible, A. P. et al. Transgenic targeting of recombinant rabies virus reveals monosynaptic connectivity of specific neurons. *J. Neurosci.* **30**, 16509–16513 (2010).
- Wickersham, I. R. et al. Monosynaptic restriction of transsynaptic tracing from single, genetically targeted neurons. *Neuron* **53**, 639–647 (2007).
- Luo, L., Callaway, E. M. & Svoboda, K. Genetic dissection of neural circuits: a decade of progress. *Neuron* **98**, 865 (2018).
- Li, E. et al. Anterograde transneuronal tracing and genetic control with engineered yellow fever vaccine YFV-17D. *Nat. Methods* **18**, 1542–1551 (2021).
- Zingg, B. et al. AAV-mediated anterograde transsynaptic tagging: mapping corticocollicular input-defined neural pathways for defense behaviors. *Neuron* **93**, 33–47 (2017).
- Zingg, B., Peng, B., Huang, J., Tao, H. W. & Zhang, L. I. Synaptic specificity and application of anterograde transsynaptic AAV for probing neural circuitry. *J. Neurosci.* **40**, 3250–3267 (2020).
- Roberts, R. W. & Szostak, J. W. RNA-peptide fusions for the in vitro selection of peptides and proteins. *Proc. Natl Acad. Sci. USA* **94**, 12297–12302 (1997).
- Gross, G. G. et al. Recombinant probes for visualizing endogenous synaptic proteins in living neurons. *Neuron* **78**, 971–985 (2013).
- Batori, V., Koide, A. & Koide, S. Exploring the potential of the monobody scaffold: effects of loop elongation on the stability of a fibronectin type III domain. *Protein Eng.* **15**, 1015–1020 (2002).
- Miesenböck, G., De Angelis, D. A. & Rothman, J. E. Visualizing secretion and synaptic transmission with pH-sensitive green fluorescent proteins. *Nature* **394**, 192–195 (1998).
- Vassar, R. et al. Beta-secretase cleavage of Alzheimer's amyloid precursor protein by the transmembrane aspartic protease BACE. *Science* **286**, 735–741 (1999).
- Gotzke, H. et al. The ALFA-tag is a highly versatile tool for nanobody-based bioscience applications. *Nat. Commun.* **10**, 4403 (2019).

23. Perez, E. E. et al. Establishment of HIV-1 resistance in CD4⁺ T cells by genome editing using zinc-finger nucleases. *Nat. Biotechnol.* **26**, 808–816 (2008).
24. Anastasiades, P. G. & Carter, A. G. Circuit organization of the rodent medial prefrontal cortex. *Trends Neurosci.* **44**, 550–563 (2021).
25. Benavidez, N. L. et al. Organization of the inputs and outputs of the mouse superior colliculus. *Nat. Commun.* **12**, 4004 (2021).
26. Zhuang, J. et al. Laminar distribution and arbor density of two functional classes of thalamic inputs to primary visual cortex. *Cell Rep.* **37**, 109826 (2021).
27. Cruz-Martin, A. et al. A dedicated circuit links direction-selective retinal ganglion cells to the primary visual cortex. *Nature* **507**, 358–361 (2014).
28. Gerfen, C. R. The neostriatal mosaic: multiple levels of compartmental organization. *Trends Neurosci.* **15**, 133–139 (1992).
29. Khibnik, L. A., Tritsch, N. X. & Sabatini, B. L. A direct projection from mouse primary visual cortex to dorsomedial striatum. *PLoS ONE* **9**, e104501 (2014).
30. Roth, B. L. DREADDs for neuroscientists. *Neuron* **89**, 683–694 (2016).
31. Queiroz Zetune Villa Real, K. et al. A versatile synaptotagmin-1 nanobody provides perturbation-free live synaptic imaging and low linkage-error in super-resolution microscopy. *Small Methods* **7**, e2300218 (2023).
32. O'Connor, E. C. et al. Accumbal D1R neurons projecting to lateral hypothalamus authorize feeding. *Neuron* **88**, 553–564 (2015).
33. Tsai, N. Y. et al. Trans-Seq maps a selective mammalian retinotectal synapse instructed by Nephronectin. *Nat. Neurosci.* **25**, 659–674 (2022).
34. Beier, K. T. et al. Anterograde or retrograde transsynaptic labeling of CNS neurons with vesicular stomatitis virus vectors. *Proc. Natl Acad. Sci. USA* **108**, 15414–15419 (2011).
35. Lo, L. & Anderson, D. J. A Cre-dependent, anterograde transsynaptic viral tracer for mapping output pathways of genetically marked neurons. *Neuron* **72**, 938–950 (2011).
36. Lin, K. et al. A mutant vesicular stomatitis virus with reduced cytotoxicity and enhanced anterograde trans-synaptic efficiency. *Mol. Brain* **13**, 45 (2020).
37. Sun, L. et al. Differences in neurotropism and neurotoxicity among retrograde viral tracers. *Mol. Neurodegener.* **14**, 8 (2019).
38. Daigle, T. L. et al. A suite of transgenic driver and reporter mouse lines with enhanced brain-cell-type targeting and functionality. *Cell* **174**, 465–480 e422 (2018).
39. Xu, W. & Sudhof, T. C. A neural circuit for memory specificity and generalization. *Science* **339**, 1290–1295 (2013).
40. Zhang, Y. et al. Fast and sensitive GCaMP calcium indicators for imaging neural populations. *Nature* **615**, 884–891 (2023).
41. Sun, F. et al. Next-generation GRAB sensors for monitoring dopaminergic activity in vivo. *Nat. Methods* **17**, 1156–1166 (2020).
42. Liu, X. et al. Optogenetic stimulation of a hippocampal engram activates fear memory recall. *Nature* **484**, 381–385 (2012).
43. Faust, T. E., Gunner, G. & Schafer, D. P. Mechanisms governing activity-dependent synaptic pruning in the developing mammalian CNS. *Nat. Rev. Neurosci.* **22**, 657–673 (2021).

Publisher's note Springer Nature remains neutral with regard to jurisdictional claims in published maps and institutional affiliations.

Open Access This article is licensed under a Creative Commons Attribution-NonCommercial-NoDerivatives 4.0 International License, which permits any non-commercial use, sharing, distribution and reproduction in any medium or format, as long as you give appropriate credit to the original author(s) and the source, provide a link to the Creative Commons licence, and indicate if you modified the licensed material. You do not have permission under this licence to share adapted material derived from this article or parts of it. The images or other third party material in this article are included in the article's Creative Commons licence, unless indicated otherwise in a credit line to the material. If material is not included in the article's Creative Commons licence and your intended use is not permitted by statutory regulation or exceeds the permitted use, you will need to obtain permission directly from the copyright holder. To view a copy of this licence, visit <http://creativecommons.org/licenses/by-nc-nd/4.0/>.

© The Author(s) 2025

Methods

AF production

Amino acids 1–394 of GluA1 grown in *Sf9* (*Spodoptera frugiperda*) cells was used as a target for an mRNA display selection, carried out as described in ref. 44. FingRs amplified from the ninth round of selection were fused to a Myc tag and coexpressed in Cos7 cells (ATCC, CRL-1651) with ss-GluA1-HA (ss, signal sequence of GluA1) and Stargazin-V5. Cos7 cells were stained live with anti-MYC antibody, then fixed, permeabilized and stained for HA and V5. Fibronectins labeling the surface of cells expressing GluA1 and Stargazin were then expressed in dissociated cultures. Fibronectin 9.3-labeled endogenous GluA1 and was designated AF.

Plasmid constructs

The ss-AF-YFP consists of DNA encoding amino acids 1–18 of *GluA1* inserted upstream of AF and yellow fluorescent protein (YFP). For ATLAS constructs, *VAMP2* complementary DNA (cDNA) was inserted upstream of ALFA-tag (SRLEEELRRRLTE) followed by a BACEcs (β -site Amyloid Precursor Protein-cleaving enzyme 1) cut site (EISEVN-LDAEFR). *VAMP2*-BACEcs-SEP has SEP downstream of BACEcs. *VAMP2*-BACEcs-AF-SEP has AF and SEP downstream of BACEcs. ATLAS_{Cre} has AF and *Cre* cDNA downstream of BACEcs. DIO-ATLAS_{Fip} has a Myc tag (EQKLISEEDL) followed by *FLPI* cDNA downstream of BACEcs and nested LoxP sites on either side of the coding sequence. GFP-HA-BACE1 plasmid was purchased (Addgene, no. 165032), and GFP was removed to make BACE-HA. The above sequences were ligated into a pAAV plasmid containing the human synapsin (hsyn) promoter and a woodchuck hepatitis virus posttranscriptional regulatory element (WPRE). Lenti-hsyn-Cre was purchased from Addgene (no. 86641), and the *hSYN1* promoter was replaced with the *CamKII α* promoter to generate Lenti-CamKII-Cre.

Dissociated cultures

Pups from timed pregnant Sprague Dawley rats (E19) were used for cultured cortical neurons, prepared as in ref. 45. All procedures were approved by the Institutional Animal Care and Use Committee of the University of Southern California.

Protein purification

Human embryonic kidney 293T cells were transfected with the plasmid pCAG-ss-AF-3XHA-TEVcs-HALOTag and the secreted protein AF-HA-TEVcs-HALOTag was collected and incubated with HaloLink resin (Promega, cat. no. G1914) overnight at 4 °C. and then with tobacco etch virus (TEV) protease (New England Biolabs, cat. no. P8112S) overnight at 4 °C. Supernatant was collected and incubated with NEBExpress Ni Resin (New England Biolabs, cat. no. S1428S) overnight at 4 °C to remove the TEV protease. Purified protein was dialyzed into 20 mM HEPES, 250 mM NaCl pH 7.4 and concentrated using the Amicon Ultra centrifugal filters (cat. no. UFC501096).

Endocytosis

Neuronal cultures were incubated with 1 mM purified AF-HA protein for 1 h at 37 °C. Next, cultures were washed three times with 1× Hanks Balanced Salt Solution containing 10 mM HEPES, fixed with 4% paraformaldehyde and stained for anti-HA (Cell Signaling, cat. no. 3724S) and anti-Map2 (Abcam, cat. no. ab5392).

Presynaptic release

Plasmids encoding *VAMP2*-BACEcs-SEP (1 μ g) or *VAMP2*-BACEcs-AF-SEP (1 μ g) with BACE-HA (2 μ g) were transfected into 15–18 day in vitro (DIV) cultured neurons. Two days before transfection, cultures were infected with AAV8-Cre and AAV8-DIO-PSD-95. FingR-TdTomato to label postsynaptic sites. Neurons were imaged 3 to 5 days later with or without 100 mM KCl. Time-lapse imaging was performed for either 100 or 200 frames at an interval of 1,000 ms and an exposure of 500 ms.

Time constants were measured using curve fitting functions in GraphPad Prism. Videos of SEP release events were generated using ImageJ by taking the difference of adjacent image frames to eliminate background and SEP fluorescence beyond the initial frame after release.

Viruses

The following viruses were purchased from Addgene: AAV8-hSyn-DIO-mCherry no. 50459, AAV8-EF1a-fDIO-mCherry no. 114471, AAV8-hsyn-DIO-eGFP no. 50457 and AAV8.hSyn.hM3D.mCherry no. 50474. All other viruses were generated in the Arnold laboratory using standard methods.

Transsynaptic tracing in culture

Neuronal cultures (14 DIV) were transfected with plasmids for ATLAS (1 μ g) and BACE-HA (2 μ g) using the calcium phosphate method. Transfection was followed immediately by infection with AAV8-hsyn-DIO-GFP and incubated for 7 days. Neurons were fixed and probed as described.

Immunocytochemistry for dissociated cultures

Neurons were stained using: anti-GFP, 1:10,000, Aves GFP-1020; anti-MYC, 1:1,000, Novus Biologicals NB600-334; anti-Map2, 1:1,000, Abcam ab5392; anti-clathrin, 1:1,000, GeneTex GTX80218; anti-mCherry, 1:1,000, Rockland M11217; anti-RFP, 1:1,000, Invitrogen MA5-15257; anti-GluA1, 1:1,000, EMD Millipore ABN241; anti-PSD-95, 1:3,000, NeuroMab 75-348; anti-HA, 1:1,000, Cell Signaling 3724S; anti-Cre, 1:1,000, EMD Millipore MAB3120; Alexa Fluor 488 goat anti-chicken, 1:1,000, Invitrogen A-11006; Alexa Fluor 594 goat anti-rabbit, 1:1,000, Invitrogen A-11012; Alexa Fluor 594 goat anti-mouse, 1:1,000, Invitrogen A-11005; Alexa Fluor 647 goat anti-mouse, 1:1,000, Invitrogen A-21235; Alexa Fluor 647 goat anti-rabbit, 1:1,000, Invitrogen A-21244; JF549 halotag ligand, 1:1,000, Janelia Farm; JF647 halotag ligand, 1:1,000, Janelia Farm; FluoTag-X2 anti-alfa 647, 1:1,000, NanoTag biotechnologies N1502 AF647. Neurons were mounted using Dapi-fluoromount-G (Electron Microscopy Services, 17984-24).

Electrophysiology (testing of AF)

All experiments were performed in accordance with National Institutes of Health (NIH) Guidelines for the Care and Use of Laboratory Animals, and all procedures were approved by the Institutional Animal Care and Use Committee of the University of Southern California. As previously described, 400- μ m-thick rat organotypic hippocampal slice cultures were prepared from male and female P6 to P8 Sprague Dawley rats⁴⁶. Sparse biolistic transfections were performed on DIV1 as previously described^{47,48}. Next, 50 μ g of mixed plasmid DNA encoding ss-AF-YFP was coated on 1- μ m diameter gold particles. Construct expression was confirmed by YFP epifluorescence. Dual whole-cell recordings of CA1 pyramidal neurons were performed on DIV7–8 through simultaneous recordings from a transfected neuron and a neighboring, nontransfected control neuron. Synaptic responses were evoked by stimulating with a monopolar glass electrode filled with artificial cerebrospinal fluid (ACSF) in the stratum radiatum. AMPAR-evoked EPSCs (-eEPSCs) were measured at -70 mV. NMDAR-eEPSCs were measured at +40 mV and were temporally isolated by measuring amplitudes 150 ms after the stimulus. For paired-pulse facilitation, paired pulses at 40-ms interpulse interval were delivered and the ratio of peak amplitudes was analyzed to generate barplots depicting mean \pm s.e.m. Data analysis was performed using Igor Pro v.9.

Animal preparation and stereotaxic surgery (mouse)

All procedures in Figs. 3, 4b–d, 5 and 6c,d and Extended Data Figs. 3, 5, 6, 7a,b, 8 and 9 were performed in accordance with NIH Guidelines for the Care and Use of Laboratory Animals and were approved by the Animal Care and Use Committee at the University of Southern California. Male and female wild-type mice (C57BL/6J, Jackson Laboratories,

strain no. 000664), *Vipr2-Cre* (*Cre* expression in dLGN, Jackson Laboratories, strain no. 031332) and *Sst-IRES-Cre* (*Cre* expression in somatostatin interneurons, Jackson Laboratories strain no. 013044) mice aged 2–6 months were used. For stereotaxic viral injection, mice were anesthetized in an induction chamber containing 4% isoflurane mixed with oxygen and transferred to a stereotaxic frame with a heating pad. Then, 1.5% isoflurane was delivered throughout the procedure through a nose cone at a rate of 0.5 l min⁻¹. Injection coordinates based on ref. 49 were used to mark the location where a small hole (0.5 mm diameter) was drilled. Viruses were delivered through pulled glass micropipettes using pressure injection via a micropump. Total injection volumes ranged from 50 to 800 nl, at 20–60 nl min⁻¹. Following injection, the micropipette was left in place for 15 min to minimize virus diffusion into the pipette track. Animals were administered Ketoprofen (5 mg kg⁻¹) at the beginning of the surgical procedure and again every 24 h for 2 d following surgery.

Injections of viruses (mouse)

For experiments in Figs. 3, 4b–d, 5, 6c,d and Extended Data Figs. 3, 5, 6, 7a,b, 8 and 9, anterograde tracing experiments using *ATLAS_{Cre}*, 400–600 nl of either *ATLAS_{Cre}* or *ATLAS_{SnCre}* virus was injected into presynaptic cells in the PFC, Primary auditory cortex (A1) or entorhinal cortex. *AAV8-DIO* reporter virus (400–800 nl), diluted to minimize the background signal, was injected into postsynaptic cells in the Str, ipsilateral claustrum, bilateral inferior colliculus or ipsilateral dentate gyrus. The animals were euthanized 2 weeks following the injections.

In experiments with *DIO-ATLAS_{Flp}*, transgenic *VIPR2-Cre* mice were injected with *AAV8-DIO-ATLAS_{Flp}* (600 nl, 1.0×10^{13}) at the ipsilateral LGN. A second injection of *AAV8-EF1a-fDIO-mCherry* (600 nl, 5.0×10^{12}) was administered at the primary visual cortex (V1). The animals were euthanized after 2 weeks. To test *AAV-DIO-ATLAS_{Flp}*, *C57BL/6J* mice were injected with a viral mixture of *AAV8-DIO-ATLAS_{Flp}* and *Lenti-hsyn-Cre* at V1 and *AAV8-EF1a-fDIO-mCherry* (600 nl, 5.0×10^{12}) in the ipsilateral SC and euthanized 2 weeks later. Transgenic *SST-Cre* mice were injected with a mixture of *AAV8-DIO-ATLAS_{Flp}* and *AAV8-ef1a-fDIO-mCherry* (at 1:1 ratio based on viral particles) at V1 and euthanized 1 week later.

For testing the potential retrograde spread of *ATLAS*, *AAV8-DIO-ATLAS_{Flp}* and *Lenti-hsyn-Cre* were injected into Str of *C57BL/6J* mice, and *AAV8-EF1a-fDIO-mCherry* (800 µl, 5.0×10^{12}) was injected into mPFC. As the negative control, a group of *C57BL/6J* mice was injected with *AAV8-ef1a-fDIO-mCherry* (800 µl, 5.0×10^{12}) in mPFC. All animals were then euthanized 2 weeks following the injections.

To test for monosynaptic tracing, *C57BL/6J* mice were injected with *AAV8-ATLAS_{Cre}* (600 nl, 1.0×10^{13}) in V1 and *AAV8-hsyn-DIO-mCherry* (400 nl, 1.0×10^{13}) in the PBG. As the positive control, *C57BL/6J* mice were injected with *AAV8-ATLAS_{Cre}* (600 nl, 1.0×10^{13}) in SC and *AAV8-hsyn-DIO-mCherry* (400 nl, 1.0×10^{13}) in PBG. As a negative control, wild-type mice were injected with *AAV8-hsyn-DIO-mCherry* (400 nl, 1.0×10^{13}) at PBG. Animals were euthanized 2 weeks following injections.

To test supplementing *ATLAS* with *BACE*, mixtures with the following ratios of *AAV8-ATLAS_{Cre}* and *AAV8-hsyn-BACE-HA*: 1:1 *ATLAS*: *BACE*, 1:5 *ATLAS*: *BACE*, or no *BACE* based on number of viral particles. These were injected into the *C57BL/6J* mice in mPFC. *AAV8-hsyn-DIO-GFP* (800 nl, 1.0×10^{13}) in ipsilateral Str to visualize postsynaptic cells. Animals were euthanized 2 weeks following injections. To examine the effect of incubation time on efficiency of *ATLAS*, *C57BL/6J* mice were injected with a viral mixture of *AAV8-ATLAS_{SnCre}* and *AAV8-hsyn-BACE-HA* (600 nl, 1:3 based on viral particles) in mPFC and *AAV8-hsyn-DIO-GFP* (800 nl, 1.0×10^{13}) in ipsilateral Str. Animals were euthanized 4, 7, 14 or 21 days following injections.

For testing the effect of neuronal activity on *ATLAS* tracing, *C57BL/6J* mice were injected with *AAV8-ATLAS_{SnCre}* or *AAV8-ATLAS_{Cre}*, *AAV8-hsyn-BACE* and *AAV8-hHM3Dq-mCherry* (600 nl, 1:3:1 based on viral particles) in mPFC and *AAV8-hsyn-DIO-GFP* (800 nl, 1.0×10^{13}) in

ipsilateral Str. *CNO* (200 µl, 1.1 mM) was administered to experiment animals through intraperitoneal injection daily following viral injections. Animals were euthanized 7 days after viral injections. A final dose of *CNO* was administered 45 min before the perfusion.

To determine whether *ATLAS* shows toxicity compared to *ATLAS_{Sn}*, one group of *C57BL/6J* mice were injected with 600 nl of *AAV8-ATLAS_{Cre}* and *AAV8-hsyn-BACE* (1:3 based on viral particles), and the other group of mice were injected with 600 nl of viral mixture of *AAV8-ATLAS_{SnCre}* and *AAV8-hsyn-BACE* (at a 1:3 ratio based on viral particles) at mPFC. *AAV8-hsyn-DIO-GFP* (800 nl) was injected into the ipsilateral Str of both groups. Animals were euthanized 14 and 28 days following injections.

In all experiments listed above, presynaptic and postsynaptic injections were performed during the same surgery. Bregma and Lambda coordinates are in millimeters as follows: anteroposterior is the distance from Lambda, mediolateral is the distance from midline and dorsoventral is the distance from Lambda except for V1, A1 and SC, which use the distance from the surface of the cortex. mPFC (6.3, 0.3, 1.7); Str (5.1, 1.8, 3.4); dLGN (2.2, 2.2, 2.9); primary visual cortex (V1) (0.8, 2.4, 0.6); primary auditory cortex (A1) (1.5, 4.2, 0.6); SC (0.6, 0.8, 1.2); inferior colliculus (−0.7, 0.8, 0.6); PBG (0.1, 1.8, 3.3); claustrum (5.4, 2.5, 4.0); entorhinal cortex (0.0, 3.6, 3.6) and dentate gyrus (0.6, 2.8, 2.5).

Histology (mouse)

Mouse brains were perfused with 40 ml of phosphate-buffered saline (PBS), then 40 ml of 4% paraformaldehyde in PBS (Figs. 3, 4b–d, 5, 6c,d and Extended Data Figs. 3, 5, 6, 7a,b, 8 and 9). The brains were fixed overnight in 4% paraformaldehyde at 4°C and dehydrated in 30% sucrose solution for at least 48 h. Brains were embedded in tissue freezing medium at −45°C and sectioned to a thickness of 25–35 µm using a cryostat. For immunohistochemistry, antibodies used were: rabbit anti-RFP, Rockland (cat. no. 600-401-379), 1:1,000; chicken anti-GFP antibody, AVES (gfp-1020, cat. no. NC9510598), 1:1,000; Fluotag-X2 anti-ALFA, NanoTag (cat. no. N1502-ALFA647-L), 1:1,000; mouse anti-NeuN antibody, EMD Millipore (cat. no. MAB377), 1:1,000, c-Fos (cat. no. 9F6) Rabbit mAb, Cell Signaling Technology (cat. no. 2250T), 1:1,000; Alexa Flour 488-conjugated goat anti-chicken (A-11039) or anti-mouse IgG (cat. no. A-28175), Thermo Fisher, 1:1,000; Alexa Flour 594-conjugated anti-rabbit IgG, Thermo Fisher (cat. no. A-11012), 1:1,000; Alexa Flour 647-conjugated goat anti-mouse IgG, Thermo Fisher, 1:1,000 (cat. no. A-21235).

Quantification of transsynaptic labeling

Labeled presynaptic cells (At) and postsynaptic cells (GFP or mCherry) were counted within an identical 1-mm² region of 25-µm-thick stained sections of target regions. All sections examined were roughly equal distance from the site of *AAV* injection. We quantified cells in two representative sections, each 25 µm apart. Then, the data from the selected sections was pooled and multiplied by two to estimate the number of labeled cells within 100 µm. To account for the background expression from spontaneous recombination by the *DIO* reporter construct, we subtracted the cell counts from control experiments from those in corresponding *ATLAS* experiments. To quantify activity-dependent transsynaptic labeling, total GFP fluorescence minus background was measured identically in Str in sections at equivalent distances from injection sites using ImageJ. For the *SST* experiment, At-labeled cells and mCherry-labeled cells were counted within an identical 1 mm² region of 25-µm-thick stained sections. The number of mCherry⁺ cells over the mCherry and At colabeled cells was then calculated.

Stereotaxic surgery and histology (M1 to Str and Thal)

All experiments in Fig. 6e–h were performed in accordance with NIH Guidelines for the Care and Use of Laboratory Animals, and all procedures were approved by the Institutional Animal Care and Use

Committee of NIH. The ATLAS_{SnCre} viral vector AAV8-SY_{Tnb}-VAM P2Δ-At-BACEs-AF-Cre and AAV8-BACE-GFP (1:1, 200 nl) were injected stereotactically into the motor cortex of wild-type mice at (1.0, 2.0, 1.8) (Fig. 4e–h). They also received an injection of a Cre-dependent reporter vector: AAV8-Ef1a-FLEX-tdTomato (Addgene, 28306) into the Str (0.5, 2.0, 4.0) and thalamus (−1.55, 1.5, 3.75). Following a survival time of 2 weeks, animals were perfused and 50-μm sections were cut with a freezing microtome. The following antibodies were used for immunocytochemistry: rabbit anti-RFP (cat. no. 600-401-379, Rockland Immunochemicals), chicken anti-GFP (cat. no. A10262, Invitrogen), goat anti-chicken 488 (cat. no. A32931, Invitrogen) and goat anti-rabbit 555 (cat. no. A32732, Invitrogen). Sections were counterstained with NeuroTrace Blue 435 (cat. no. N21479, Invitrogen) and coverslipped with Aqua-polymount (cat. no. 18606, Polysciences). Slides with 12–15 coronal brain sections were imaged on a Zeiss EpiFluorescence Microscope equipped with Xylis broad spectrum LED illumination (Excelitas Technologies), a Hammamatsu Orca Flash4.0 camera and Ludl stage drive controlled by Neurolucida 360 Imaging software (MBF Bioscience). Images were registered using NeuroInfo v.2022.1.1.

Animal preparation and stereotaxic surgery (rat)

All experiments were performed in accordance with NIH Guidelines for the Care and Use of Laboratory Animals, and all procedures were approved by the Institutional Animal Care and Use Committee of the University of Southern California. Male Sprague Dawley rats (Envigo) weighing 300–400 g were injected with viruses delivered using a micro-infusion pump (Harvard Apparatus) connected to a 33-gauge microsyringe injector attached to a PE20 catheter and Hamilton syringe. Flow rate was 5 μl min^{−1}. Injectors were left in place for 3 min postinjection. Viruses were incubated for 21 days after injection. AAV8-ATLAS_{SnCre} was unilaterally injected into the CA1v at: −4.9 mm anteroposterior, ±4.8 mm mediolateral, −7.8 mm dorsoventral (zeroing at skull site). AAV-pCAG-FLEX-tdTomato-WPRE (Addgene; cat. no. 51503) was unilaterally injected into the ACB: +1.2 mm anteroposterior, ±1.0 mm mediolateral, −6.75 mm dorsoventral (zeroing at dura). Injection volume was 100 nl per site. For control experiments animals were injected with AAV-pCAG-FLEX-tdTomato-WPRE unilaterally in the ACB, but no injection was made in the ventral CA1. Photomicrographs were acquired using a Nikon 80i (Nikon DS-QI1, 1,280 × 1,024 resolution, 1.45 megapixel) microscope under epifluorescence controlled by NIS-Elements v.C6.10.01.

Histology (rat)

Following perfusion and fixation, Brains were sectioned into 30-μm sections on a microtome cooled with dry ice, collected in an antifreeze solution and stored in a −20 °C freezer. The following antibodies were used for immunocytochemistry: Rabbit anti-RFP (1:2,000, Rockland Inc.; cat. no. 600-401-379; Clonality: Polyclonal) and FluoTag-X2 anti-ALFA (1:1,000, NanoTag Biotechnologies; cat. no. N1502).

Quantification of activity-dependent transsynaptic labeling

For experiments to quantify transsynaptic labeling with and without BACE, mCherry-expressing cells were counted within an identical 1-mm² region over four consecutive 25-μm stained sections of Str. For experiments to quantify activity-dependent transsynaptic labeling, total GFP fluorescence minus background was measured identically in Str sections using ImageJ v.1.49b, Slidebook v.8 and Zen Microscopy v.3.11.

Electrophysiology (PFC to Str)

For experiments in Extended Data Fig. 4, wild-type C57BL/6J mice coinjected with AAV8-ATLAS_{SnCre}, AAV8-BACE-HA and AAV8-DIO-ChR2-GFP into the mPFC, and DIO-mCherry in Str were used for slice recording. Details of the stereotaxic surgery are the same as in Figs. 3a–d and

6c,d. Four weeks following injections, animals were decapitated following anesthesia, and the brain was rapidly removed and immersed in an ice-cold dissection buffer (composition 60 mM NaCl, 3 mM KCl, 1.25 mM NaH₂PO₄, 25 mM NaHCO₃, 115 mM sucrose, 10 mM glucose, 7 mM MgCl₂, 0.5 mM CaCl₂; saturated with 95% O₂ and 5% CO₂; pH 7.4). Coronal slices of 350 μm thickness were sectioned by a vibrating microtome (Leica VT1000s) and recovered for 30 min in a submersion chamber filled with warmed (35 °C) ACSF (composition 119 mM NaCl, 26.2 mM NaHCO₃, 11 mM glucose, 2.5 mM KCl, 2 mM CaCl₂, 2 mM MgCl₂, and 1.2 mM NaH₂PO₄, 2 mM sodium pyruvate, 0.5 mM VC). Str neurons surrounded by GFP⁺ fibers were visualized under a fluorescence microscope (Olympus BX51 WI). Patch pipettes (−4–5 MΩ resistance) filled with a cesium-based internal solution (composition 125 mM cesium gluconate, 5 mM TEA-Cl, 2 mM NaCl, 2 mM CsCl, 10 mM HEPES, 10 mM EGTA, 4 mM ATP, 0.3 mM GTP and 10 mM phosphocreatine; pH 7.25; 290 mOsm) were used for whole-cell recordings. Signals were recorded under voltage-clamp mode at a holding voltage of −70 mV for excitatory currents, filtered at 2 kHz and sampled at 10 kHz. Tetrodotoxin (1 μM) and 4-aminopyridine (1 mM) were added to the external solution for recording monosynaptic responses to blue light stimulation (5-ms pulse, 3-mW power, 5–10 trials).

Surgery (V1 to Str)

Experiments in Fig. 4e–h were performed in accordance with NIH Guidelines for the Care and Use of Laboratory Animals, and all procedures were approved by the Institutional Animal Care and Use Committee of Harvard Medical School. Injections were performed through a pulled glass at a rate of 30 nl min^{−1}. After injections, pipettes were slowly withdrawn (less than 100 μm s^{−1}) at least 5 min after the end of the infusion. Viruses were injected in two rounds of surgeries to minimize expression competition between ATLAS viruses (that is ATLAS_{SnCre}, BACE-HA) and Cre-dependent ChR2. Wild-type animals undergo the first round of surgery between 4 and 8 weeks of age (Fig. 4e–h). Before the start of surgery, presynaptic virus cocktail was prepared by mixing AAV8-hSyn-ATLAS_{SnCre} and AAV8-hSyn-BACE-HA in 3:1 ratio (titer is 2 × 10¹³ gc ml^{−1} for both viruses). During surgery, presynaptic virus cocktail was injected at three separate sites in V1. In addition, AAV8-hSyn-DIO-mCherry or AAV9-CAG-DIO-tdTomato was injected into two separate sites in Str. Then 14 days after the first surgery, AAV8-hSyn-DIO-ChR2-GFP was injected at the same three V1 sites as the first surgery.

Coordinates of V1 injection sites were as follows (coordinates are relative to bregma and dorsoventral is relative to the brain surface, below). Here, 300 nl of presynaptic virus cocktail (AAV8-ATLAS_{SnCre} and AAV8-BACE-HA) was injected per site for the first surgery. Then 200 nl of AAV8-hSyn-DIO-ChR2 was injected per site for the second surgery.

- V1 site 1: −2.75 mm anteroposterior, ±2.5 mm mediolateral, −0.65 mm dorsoventral
- V1 site 2: −3.80 mm anteroposterior, ±2.9 mm mediolateral, −0.65 mm dorsoventral
- V1 site 3: −3.80 mm anteroposterior, ±2.0 mm mediolateral, −0.65 mm dorsoventral

Next, 500 nl of postsynaptic virus (Cre-dependent mCherry or tdTomato) was injected at Str site 1 (anterior) while 400 nl of virus was injected at Str site 2 (posterior).

- Str site 1: 0.70 mm anteroposterior, ±1.60 mm mediolateral, −2.22 mm dorsoventral
- Str site 2: −0.58 mm anteroposterior, ±2.75 mm mediolateral, −2.75 mm dorsoventral

Electrophysiology (V1 to Str)

For experiments in Fig. 4e–h, brain slices were obtained from 2- to 3-month-old mice (both male and female) using standard techniques.

The experiments closely followed the procedures outlined in previous studies^{50,51}. Mice were anesthetized using isoflurane inhalation and subsequently subjected to transcardial perfusion with ice-cold ACSF composed of the following (in mM): 125 NaCl, 2.5 KCl, 25 NaHCO₃, 2 CaCl₂, 1 MgCl₂, 1.25 NaH₂PO₄ and 11 glucose (final osmolarity of 300–305 mOsm kg⁻¹). The brain was removed from the skull, placed in ice-cold ACSF and 250–300- μ m coronal brain slices were cut and initially placed in a holding chamber for 10 min at 34 °C in a choline-based solution composed of (in mM): 110 choline chloride, 25 NaHCO₃, 2.5 KCl, 7 MgCl₂, 0.5 CaCl₂, 1.25 NaH₂PO₄, 25 glucose, 11.6 ascorbic acid and 3.1 pyruvic acid. Following choline incubation, slices were transferred to a second chamber with ACSF at 34 °C for a minimum of 30 min. The chamber was subsequently shifted to room temperature for the duration of the experiment. All recordings were made within 4–5 h of slicing. The temperature was maintained at 32 °C and carbogen-bubbled ACSF was perfused at a rate of 2–3 ml min⁻¹ for all experiments.

Monosynaptically connected striatal neurons were identified by their mCherry-positive or tdTomato-positive somata. Fluorescence-negative neurons with GABAergic interneuron physiological properties (membrane tau decay <0.8 ms for both fast-spiking and persistent low-threshold spiking subtypes; input resistance >500 M Ω in persistent low-threshold spiking subtype) were excluded from the analysis.

Striatal neurons were patched in whole-cell voltage-clamp configurations using borosilicate glass electrodes (3–5 M Ω) filled with cesium-based (voltage clamp) internal solution to measure EPSCs. The solution contained (in mM): 135 CsMeSO₃, 10 HEPES, 1 EGTA, 3.3 QX-314 (Cl⁻ salt), 4 Mg-ATP, 0.3 Na-GTP, 8 Na₂-phosphocreatine, with pH adjusted to 7.3 using CsOH, resulting in an osmolarity of 295 mOsm kg⁻¹. All recorded neurons exhibited electrophysiological characteristics of spiny projection neurons. All synaptic currents were recorded with a cesium-based internal and monitored at a holding potential of -70 mV. Fluorescent positive and negative neurons were patched as randomly ordered sequential pairs, strictly within one field of view of each other. Chr2-mediated synaptic currents from V1 were optically evoked using 2-ms pulses of 473-nm light at light powers of 2 mW controlled through an acousto-optic modulator.

To assess the baseline connection probability of V1-DMS circuit viruses were injected in V1 at identical locations, titer and volume and at identical times as described above (see Surgery section for Fig. 4e–h). After 4 weeks, brain slices were obtained and patched in whole-cell voltage-clamp configurations as described above. We first found the field of view with maximal Chr2 fiber expression in DMS and randomly patched cells within it. Chr2-mediated synaptic currents from V1 were optically evoked using as above.

Quality control criteria were a stable baseline membrane resistance (variation in R_m < 10%) and a stable baseline resting potential with median standard deviation of ≤ 0.5 mV across recordings. Optically evoked EPSCs were analyzed post hoc using MATLAB v.2024a.

Statistics and reproducibility

Experiments in Fig. 1c were performed in three independent cultures; in Fig. 1d, two cultures; in Fig. 1e–g, five cultures; in Fig. 1h, four cultures; in Fig. 1n, ten slices; in Fig. 1o, eight slices; in Fig. 1p, six slices; in Fig. 2b–e, in three independent cultures. Experiments in Figs. 3l and 4b–d were performed in one mouse bilaterally and another mouse unilaterally. Experiments in Fig. 6b were performed in three cultures, in Fig. 6c–h, in three mice and in Fig. 6j–l, in three rats.

Experiments in Extended Data Figs. 1a–h and 2a–g were performed in two cultures; in Extended Data Fig. 6, in two mice; in Extended Data Fig. 7, in three mice. All values are expressed as mean \pm s.e.m.

Reporting summary

Further information on research design is available in the Nature Portfolio Reporting Summary linked to this article.

Data availability

Images used in quantifying transsynaptic experiments are available on the G-Node database at https://gin.g-node.org/Haoyangh/ATLAS_nature_method_2024.git. All original microscopic images are available on request to the corresponding author, as these images require additional annotation and context to be accurately interpreted. AAV8-ATLASn_{Cre}, AAV8-DIO-ATLASn_{Flp} and AAV-DIO-BACE-HA sequences and plasmids are available at Addgene, IDs 232351, 232352 and 232353. Source data are provided with this paper.

References

- Olson, C. A., Liao, H.-I., Sun, R. & Roberts, R. W. mRNA display selection of a high-affinity, modification-specific phospho-IkappaBalpha-binding fibronectin. *ACS Chem. Biol.* **3**, 480–485 (2008).
- Lewis, T. L. Jr., Mao, T., Svoboda, K. & Arnold, D. B. Myosin-dependent targeting of transmembrane proteins to neuronal dendrites. *Nat. Neurosci.* **12**, 568–576 (2009).
- Stoppini, L., Buchs, P. A. & Muller, D. A simple method for organotypic cultures of nervous tissue. *J. Neurosci. Methods* **37**, 173–182 (1991).
- Schnell, E. et al. Direct interactions between PSD-95 and stargazin control synaptic AMPA receptor number. *Proc. Natl Acad. Sci. USA* **99**, 13902–13907 (2002).
- Lu, W. et al. Subunit composition of synaptic AMPA receptors revealed by a single-cell genetic approach. *Neuron* **62**, 254–268 (2009).
- George Paxinos, K. F. *Paxinos and Franklin's the Mouse Brain in Stereotaxic Coordinates* 4th edn, Vol. 1 (Elsevier/Academic, 2013).
- Saunders, A. et al. A direct GABAergic output from the basal ganglia to frontal cortex. *Nature* **521**, 85–89 (2015).
- Wallace, M. L. et al. Genetically distinct parallel pathways in the entopeduncular nucleus for limbic and sensorimotor output of the basal ganglia. *Neuron* **94**, 138–152 e135 (2017).

Acknowledgements

We thank all Arnold laboratory members for helpful discussions. We also thank A. Delgadillo, A. Bareghamyan, R. Yan, X. Xi and C. McWilliam for technical assistance, and F. Wang for crucial input at the beginning stages of this project. We thank E. Liman for her insightful comments on the manuscript. From the Sabatini laboratory, we thank W. Wang, S. Tang and K. Reinhold for excellent experimental assistance and intellectual input. This work was supported by a grant from the National Institute of Mental Health (NIMH) and the Brain Initiative (grant no. MH116989) to D.B.A., NIMH IRP award (grant no. ZIA MH002497-34) to C.R.G., a grant (no. DK104897) to S.E.K. from NIDDK, by NINDS grant (no. R37NS046579) to B.L.S. and by Brain Initiative NRSA (grant no. 5F32MH125596) to A.E.G.

Author contributions

D.B.A. conceived and designed the study, assisted with data analysis and wrote the paper with input from all authors. J.F.R. generated the AF and performed the biochemistry and neuronal culture-related experiments. J.F.R. and M.Q. designed and generated the plasmid constructs. H.H., W.W. and H.S. performed and analyzed all in vivo tracing experiments in mice except for those mentioned below. J.F.R., W.W., H.S., H.H. and M.Q. generated the AAVs and lentiviruses. L.I.Z. and C.T. designed, and C.T. performed, the electrophysiology experiments in Extended Data Fig. 4a–f. A.E.G., S.L. and B.L.S. designed, and A.E.G., S.L. and M.A.A. performed, the electrophysiology experiments in Fig. 4e–h and the related experiments in Extended Data Fig. 4g,h. S.R. and B.E.H. designed, and S.R. performed, the electrophysiology experiments in Fig. 1. C.R.G. designed, and R.P. performed, the experiments in

Fig. 6e–h and Extended Data Fig. 7c–h. M.E.K. and S.E.K. designed, and M.E.K. performed, the experiments in Fig. 6i–l.

Competing interests

An international patent application (no. PCT/US2024/044732) has been filed. Inventors: D.B.A., J.F.R., H.H. and W.W. Status of application: submitted but not reviewed. The entire manuscript is covered in the patent application. The remaining authors declare no competing interests.

Additional information

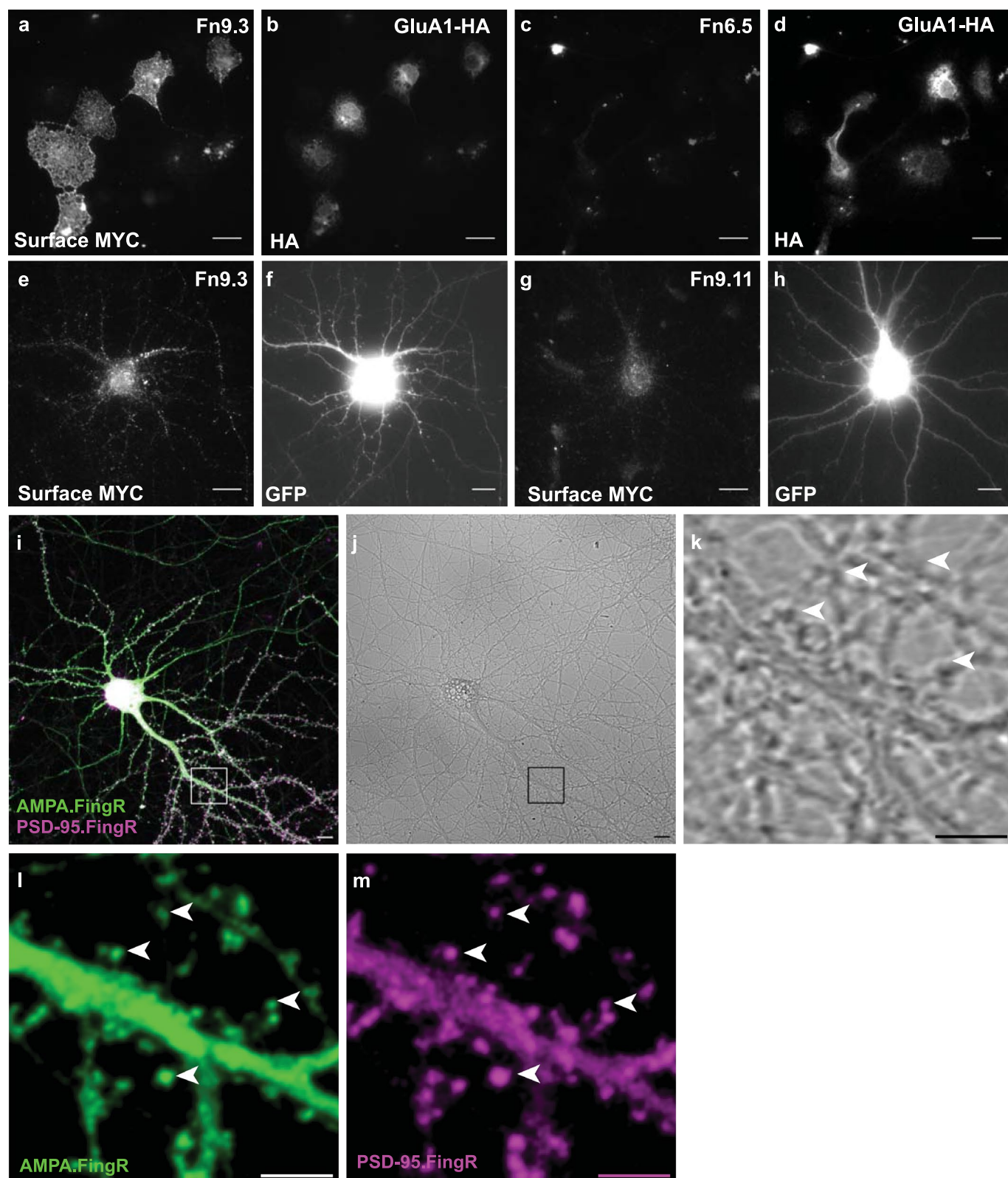
Extended data is available for this paper at <https://doi.org/10.1038/s41592-025-02670-x>.

Supplementary information The online version contains supplementary material available at <https://doi.org/10.1038/s41592-025-02670-x>.

Correspondence and requests for materials should be addressed to Don B. Arnold.

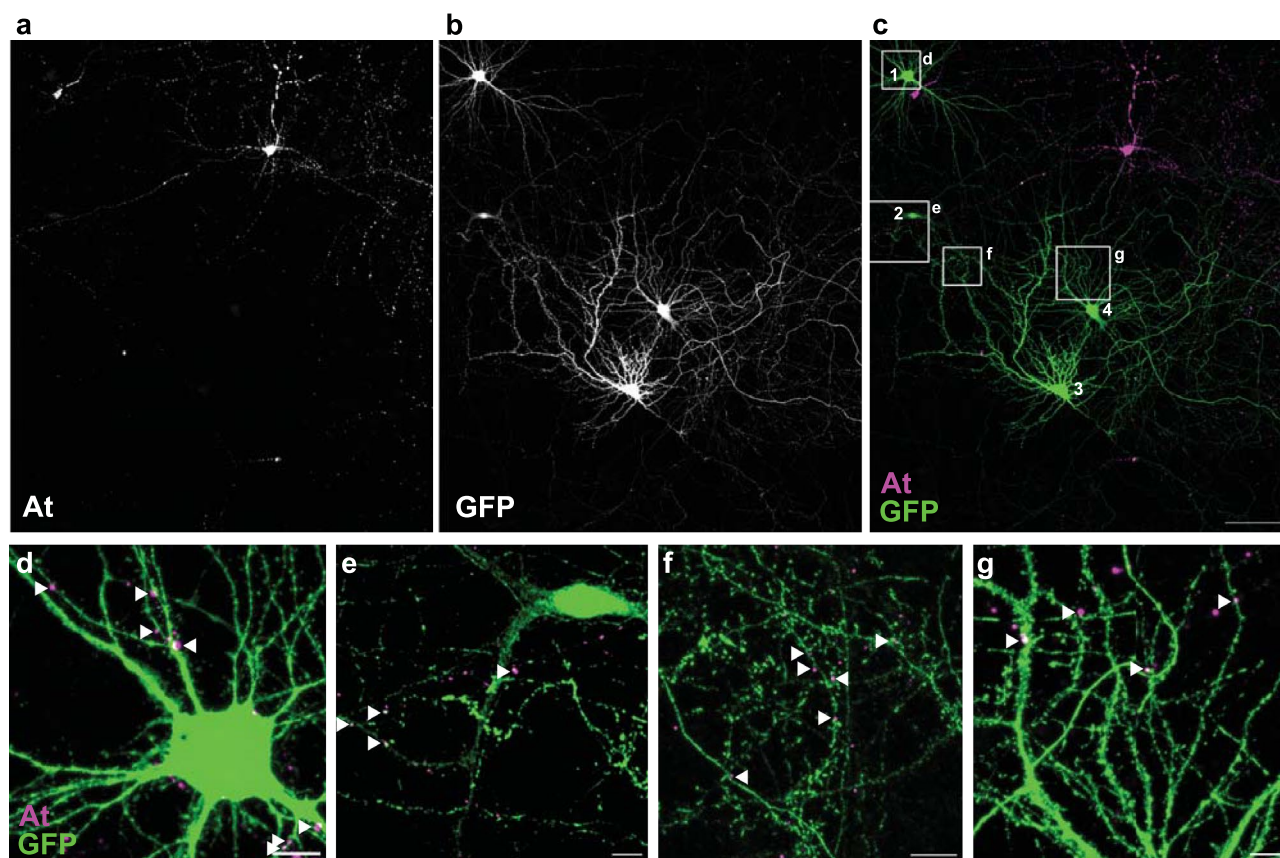
Peer review information *Nature Methods* thanks the anonymous reviewers for their contribution to the peer review of this work. Primary Handling Editor: Nina Vogt, in collaboration with the *Nature Methods* team.

Reprints and permissions information is available at www.nature.com/reprints.



Extended Data Fig. 1 | Testing of the AMPA.FingR. **a.** COS7 cells cotransfected with ss-Fn9.3-MYC, Stargazin-V5, and GluA1-HA. **b.** Permeabilized labeling of HA in same cells as in **a.** **c.** COS7 cells cotransfected with Fn6.5-MYC, Stargazin-V5, and GluA1-HA. **d.** Permeabilized labeling of HA in same cells as in **c.** **e., f.** Labeling following co-expression of ss-Fn9.3-MYC with GFP in cultured cortical neurons. **g., h.** Lack of MYC surface labeling following co-expression of ss-Fn9.11-MYC with

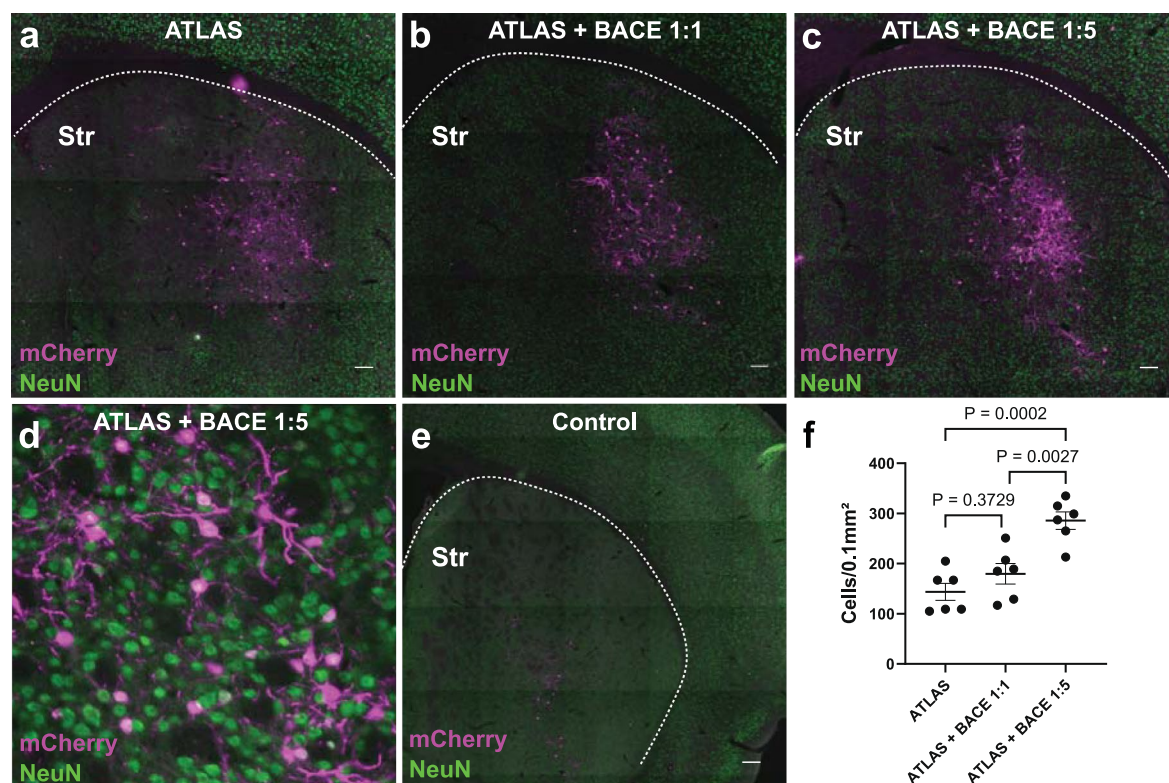
GFP in cultured cortical neurons. **i.** Live cortical neuron in culture expressing ss-AF-YFP (green) and PSD-95.FingR-tagRFP (magenta). Figure 1c is a closeup of the boxed region. **j.** DIC image of cell in **i.** **k.** Closeup of boxed area in **j.** Arrowheads point to the same synapses in **k., l.,** and **m.** **l.** Closeup of boxed area in **i.** showing ss-AF-YFP. **m.** Closeup of boxed area in **i.** showing PSD-95.FingR-tagRFP. Scale bars 20 μm in **a.-h.,** 10 μm in **i.-m.**



Extended Data Fig. 2 | Transsynaptic labeling in culture with ATLAS.

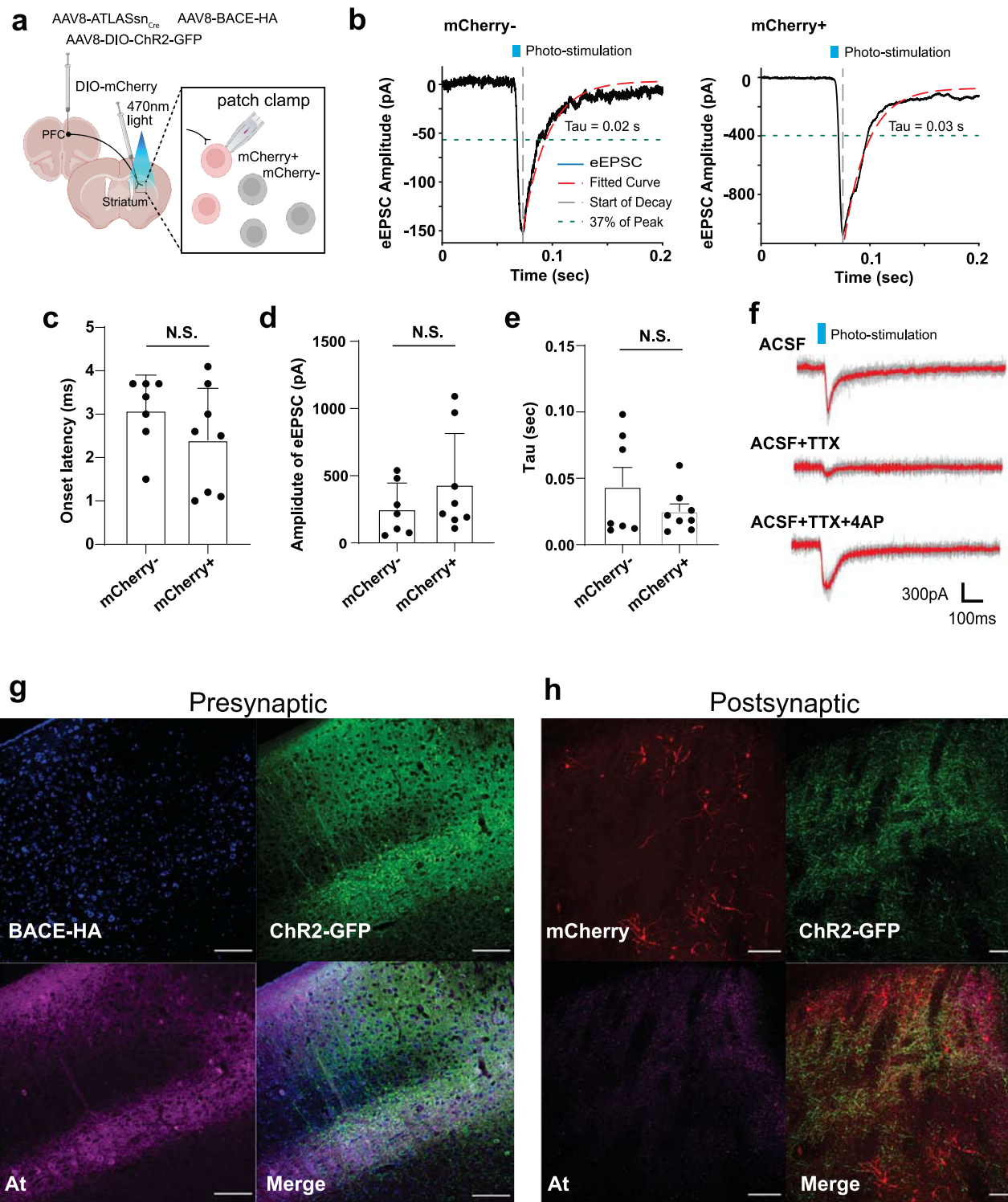
a. Presynaptic neuron labeled with At. **b.** Postsynaptic neurons labeled with GFP in same experiment as in **a.** **c.** Merge of **a.** and **b.** showing presynaptic neuron (At) labeled in magenta and postsynaptic neurons (GFP) labeled in green. **d.** Closeup of boxed region **d** from panel **c.** showing adjacent/overlapping presynaptic termini (magenta) and dendrites or spines (green) indicated by arrowhead, consistent with synaptic contacts between the presynaptic neuron in **a.** and postsynaptic neuron 1 in **c.** **e.** Closeup of boxed region **e** from panel **c.** showing adjacent/overlapping presynaptic termini (magenta) and dendrites or spines

(green) indicated by arrowhead, consistent with synaptic contacts between the presynaptic neuron in **a.** and postsynaptic neuron 2 in **c.** **f.** Closeup of boxed region **f** from panel **c.** showing adjacent/overlapping presynaptic termini (magenta) and dendrites or spines (green) indicated by arrowhead consistent with synaptic contacts between the presynaptic neuron in **a.** and postsynaptic neuron 3 in **c.** **g.** Closeup of boxed region **g** from panel **c.** showing adjacent/overlapping presynaptic termini (magenta) and dendrites or spines (green) indicated by arrowhead. Scale bars 100 μm in **c.** 10 μm in **d-g.**



Extended Data Fig. 3 | Improving the efficiency of ATLAS by co-expressing BACE. **a.** mCherry (magenta) and endogenous NeuN (green) labeling in Str in mouse brain infected with AAV8-ATLAS_{Cre} in mPFC and AAV8-DIO-mCherry in Str. **b.** Same as in **a.** with a 1:1 ratio (viral particles) of AAV8-ATLAS_{Cre}:BACE-HA injected into mPFC and AAV8-DIO-mCherry in Str. **c.** Same as in **a.** with 1:5 ratio of AAV8-ATLAS_{Cre}:BACE-HA injected into mPFC and AAV8-DIO-mCherry in the

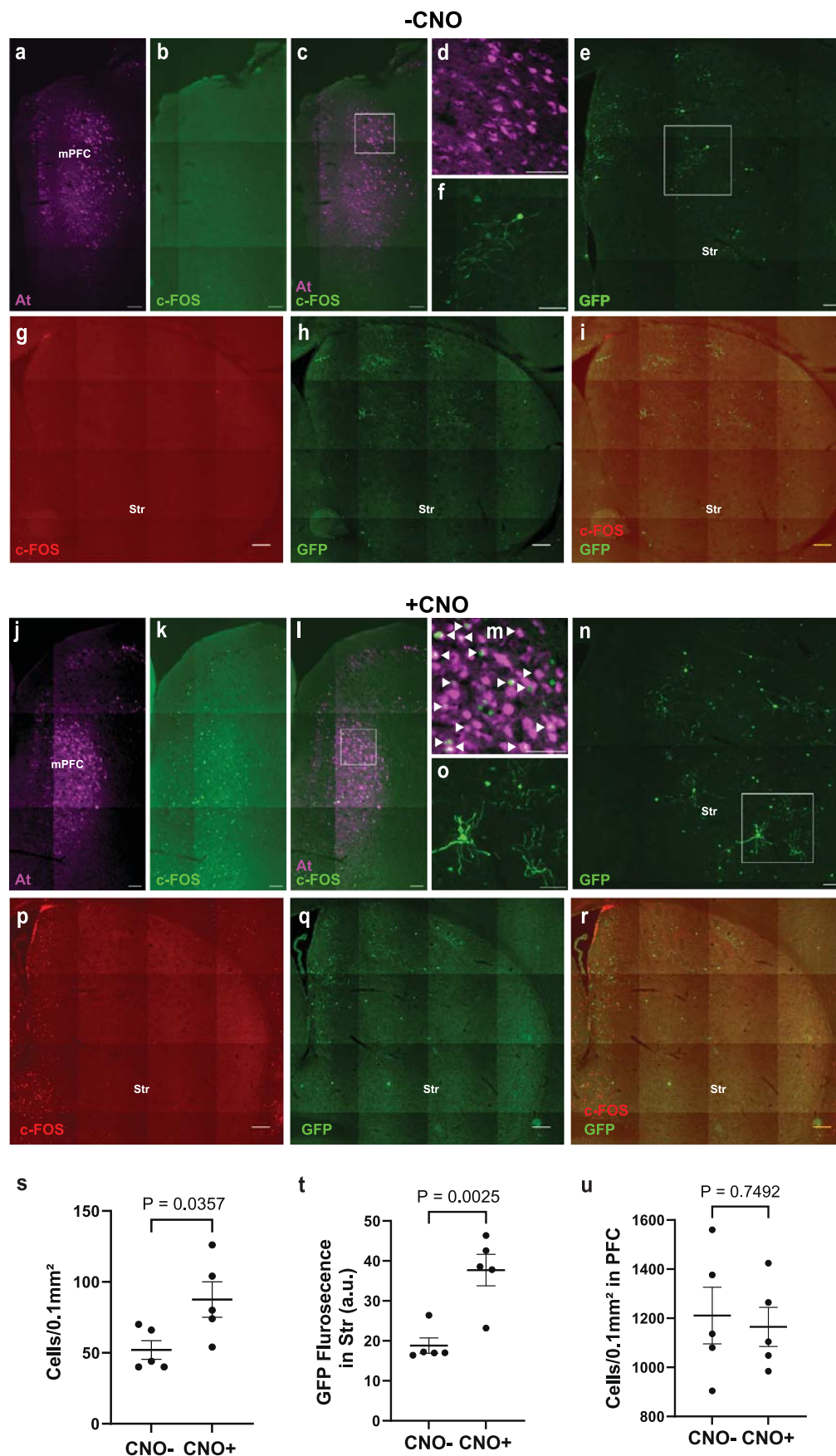
Str. **d.** Closeup of Str from same experiment as in **c.** **e.** Control staining from an experiment with an injection of AAV8-DIO-mCherry only in Str. **f.** Expressing ATLAS + BACE-HA 1:5 in mPFC leads to significantly higher labeling density in Str than ATLAS alone or ATLAS + BACE 1:1. (Tukey's multiple comparisons test). Scale bars 100 μ m.



Extended Data Fig. 4 | ATLAS tracing does not disrupt synaptic transmission.

a. Schematic of configuration for whole cell patch clamp recording from Str neurons following ATLAS-mediated tracing from mPFC. **b.** Example traces of light-evoked EPSCs from mCherry- and mCherry+ striatal neurons following optical activation of inputs from mPFC. **c.** Statistics comparing onset latency of eEPSC between mCherry- ($n = 7$ cells from 3 animals) and mCherry+ ($n = 8$ cells from 3 animals, mean \pm SEM) striatal neurons. Two-tailed unpaired t-test, N.S., $P = 0.2251$. **d.** Statistics comparing amplitudes of eEPSCs measured in mCherry- ($n = 7$ cells from 3 animals) and mCherry+ ($n = 8$ cells from 3 animals, mean \pm SEM) striatal neurons. Two-tailed unpaired t test, N.S., $P = 0.2766$. **e.** Statistics comparing time constants of eEPSCs measured in mCherry- ($n = 7$ cells from 3 animals, mean \pm SEM) and mCherry+ ($n = 8$ cells from 3 animals)

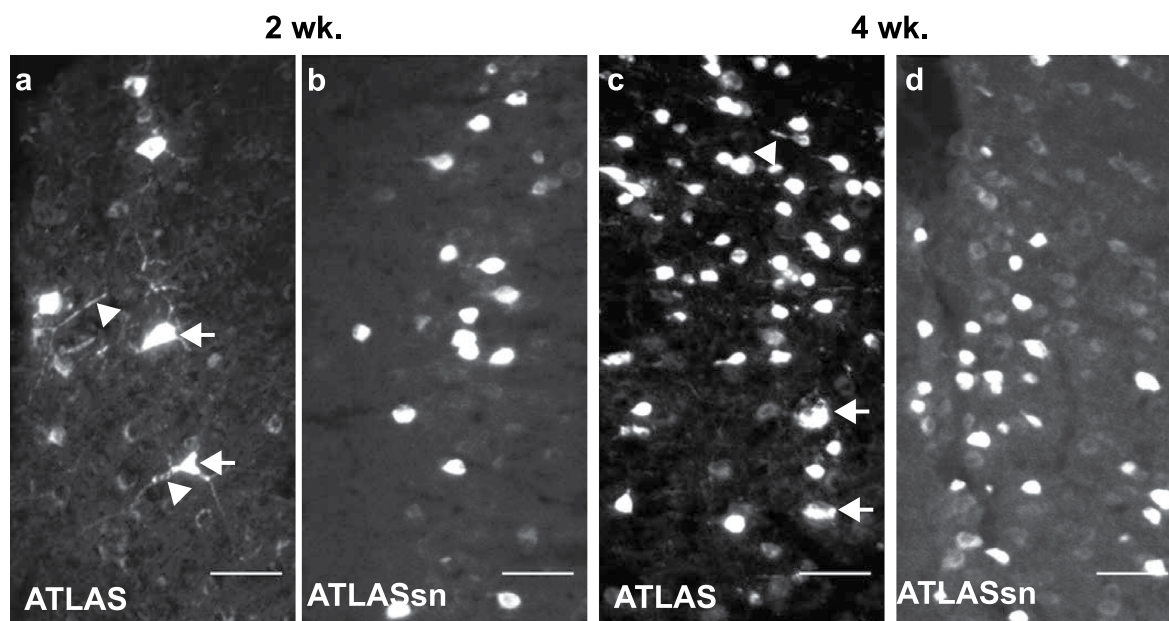
striatal neurons. Two-tailed unpaired t-test, N.S., $P = 0.2342$. **f.** Traces illustrate the monosynaptic nature of the excitatory input to mCherry-labeled striatal neurons. eEPSC was suppressed by TTX application and rescued by 4AP. **g.** High magnification histological sections showing presynaptic expression patterns in V1 of BACE (upper left), Cre-dependent ChR2 (upper right), ATLAS_{Sn_{Cre}} (At, lower left), and merged (lower right), as in experiments in Fig. 4e–h. **h.** High magnification histological sections showing postsynaptic expression patterns in the dorsomedial striatum of mCherry/tdTomato (upper left), Cre-dependent ChR2 (upper right), and ATLAS_{Sn_{Cre}} (At, lower left), and merged (lower right), as in experiments in Fig. 4e–h. Experiments in **g.** and **h.** were performed in 3 mice. Scale bars 100 μ m.



Extended Data Fig. 5 | See next page for caption.

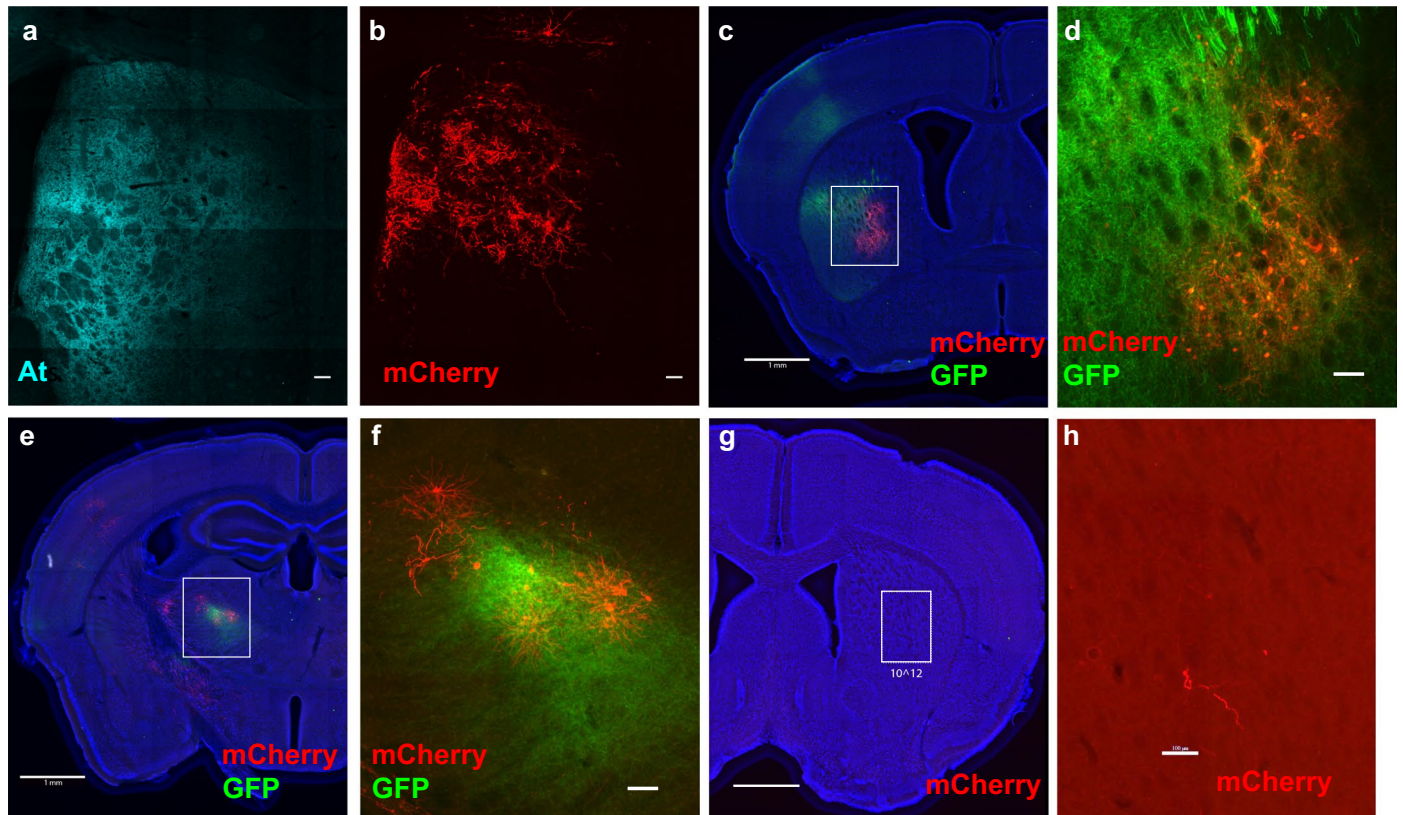
Extended Data Fig. 5 | In vivo transsynaptic labeling with ATLAS is activity-dependent. **a.** Coronal section from mPFC of mouse infected with AAV8-ATLAS_{Cre} + AAV8-hHM3Dq-mCherry in mPFC and AAV8-DIO-GFP in Str, stained after one week. **b.** Same section as in **a.** labeled for endogenous c-FOS (green). **c.** Merge of **a.** and **b.** **d.** Closeup of marked region in **c.** **e.** GFP labeling of postsynaptic cells in Str. **f.** Closeup of marked region in **e.** **g.** Str from same mouse as **a.** showing c-FOS labeling (red). **h.** Same section as **g.** showing GFP labeling. **i.** Merge of **g.** and **h.** **j.** Coronal section from mouse as in **a.** subjected to intraperitoneal injections of CNO. **k.** Same section as **j.** labeled for endogenous c-FOS. **l.** Merge of **j.** and **k.** **m.** Closeup of marked region in **l.** showing colocalization of c-FOS and At (arrowheads). **n.** GFP labeling of postsynaptic cells

in Str. **o.** Closeup of marked region in **n.** **p.** Str from same mouse as in **j.** labeled with c-FOS (red). **q.** Same section as **p.** showing GFP labeling. **r.** Merge of **p.** and **q.** **s.** Significantly more cells in Str were labeled with GFP in mice injected with CNO vs. those without ($n = 5$, unpaired t-test, two-tailed). Each data point represents a biological replicate in a different mouse. **t.** Intensity of GFP label in Str was significantly greater in mice injected with CNO vs. mice without CNO ($n = 5$, unpaired t-test, two-tailed). Each data point represents a biological replicate in a different mouse. **u.** The number of cells labeled with At in mPFC was not significantly different in mice injected with CNO vs. in mice without CNO ($n = 5$, unpaired t-test, two-tailed). Each data point represents a biological replicate in a different mouse. Scale bar 100 μm . Error bars depict mean \pm SEM.



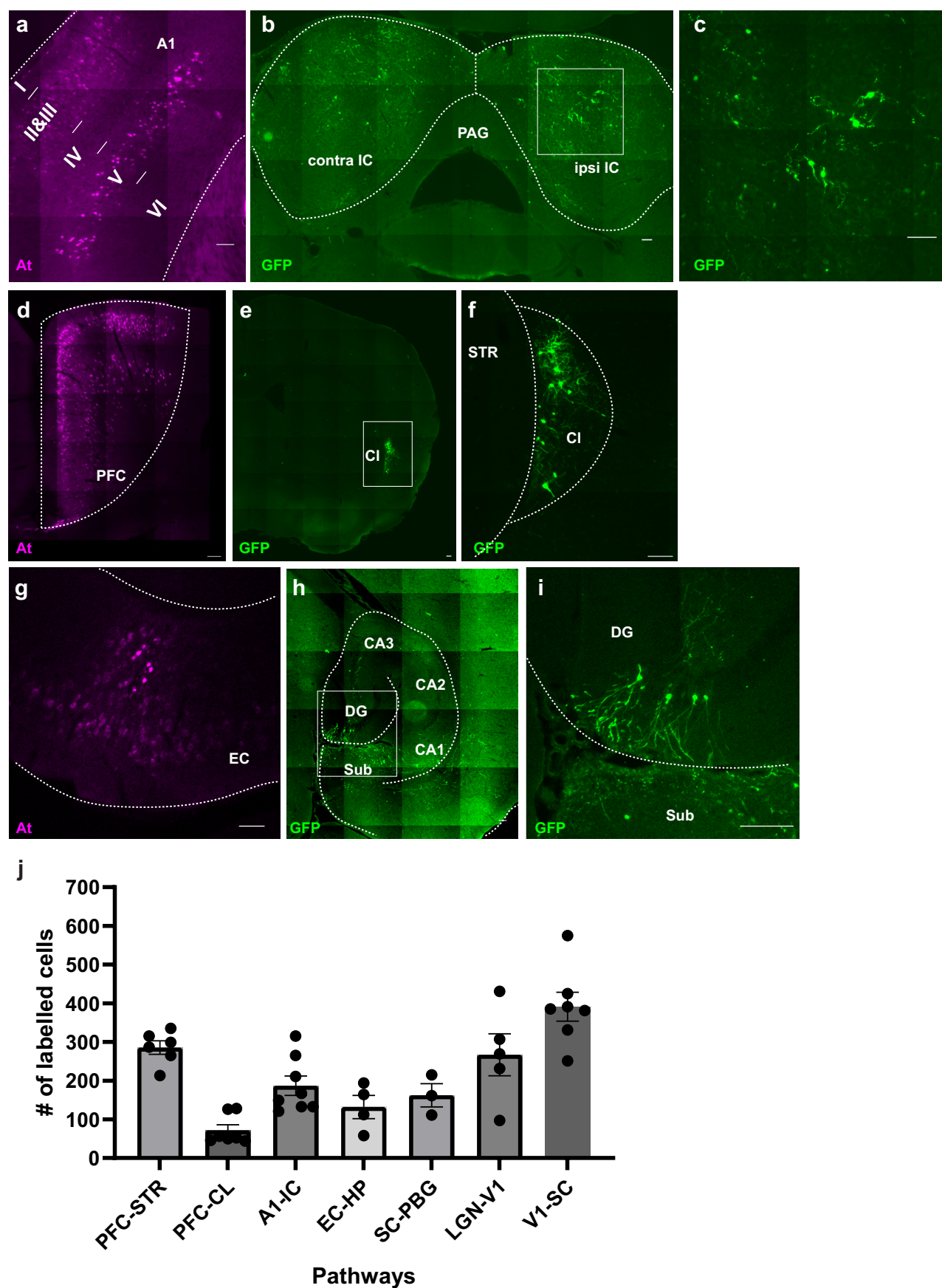
Extended Data Fig. 6 | Toxicity associated with ATLAS, but not ATLASsn.
a. Coronal section of mPFC following expression of ATLASsn_{Cre} for 2 weeks. Toxicity is evidenced by degenerating processes (arrowhead) and swollen cell bodies (arrow). Experiments were performed in two mice. **b.** Coronal section of mPFC following expression of ATLASsn_{Cre} for 2 weeks. Experiments were

performed in two mice. **c.** Same as **a.** following expression for 4 weeks. Degenerating processes (arrowhead) and swollen cell bodies (arrows) are apparent. Experiments were performed in two mice. **d.** Same as **b.** following expression for 4 weeks.



Extended Data Fig. 7 | Transsynaptic labeling of ATLASn_{Cre} from the cortex to the striatum and thalamus. **a.** Coronal section from striatum of mouse in Fig. 6c, d injected with AAV8-ATLASn_{Cre} in medial prefrontal cortex and AAV8-DIO-mCherry in the striatum and incubated for two weeks showing At labeling of presynaptic termini. **b.** Coronal section from striatum of same mouse as in **a.** showing mCherry-labeled neurons. **c.** Coronal section at the level of the striatum of mouse brain injected with AAV8-ATLASn_{Cre} + AAV8-BACE-GFP in the M1 cortex and AAV8-DIO-mCherry in the striatum and thalamus. Sections were stained for GFP (green), mCherry (red), and fluorescent Nissl stain (blue). **d.** Closeup of area marked in **c.** showing overlap of projections from neurons expressing AAV8-BACE-GFP (green) and neurons expressing mCherry. **e.** Coronal section at the

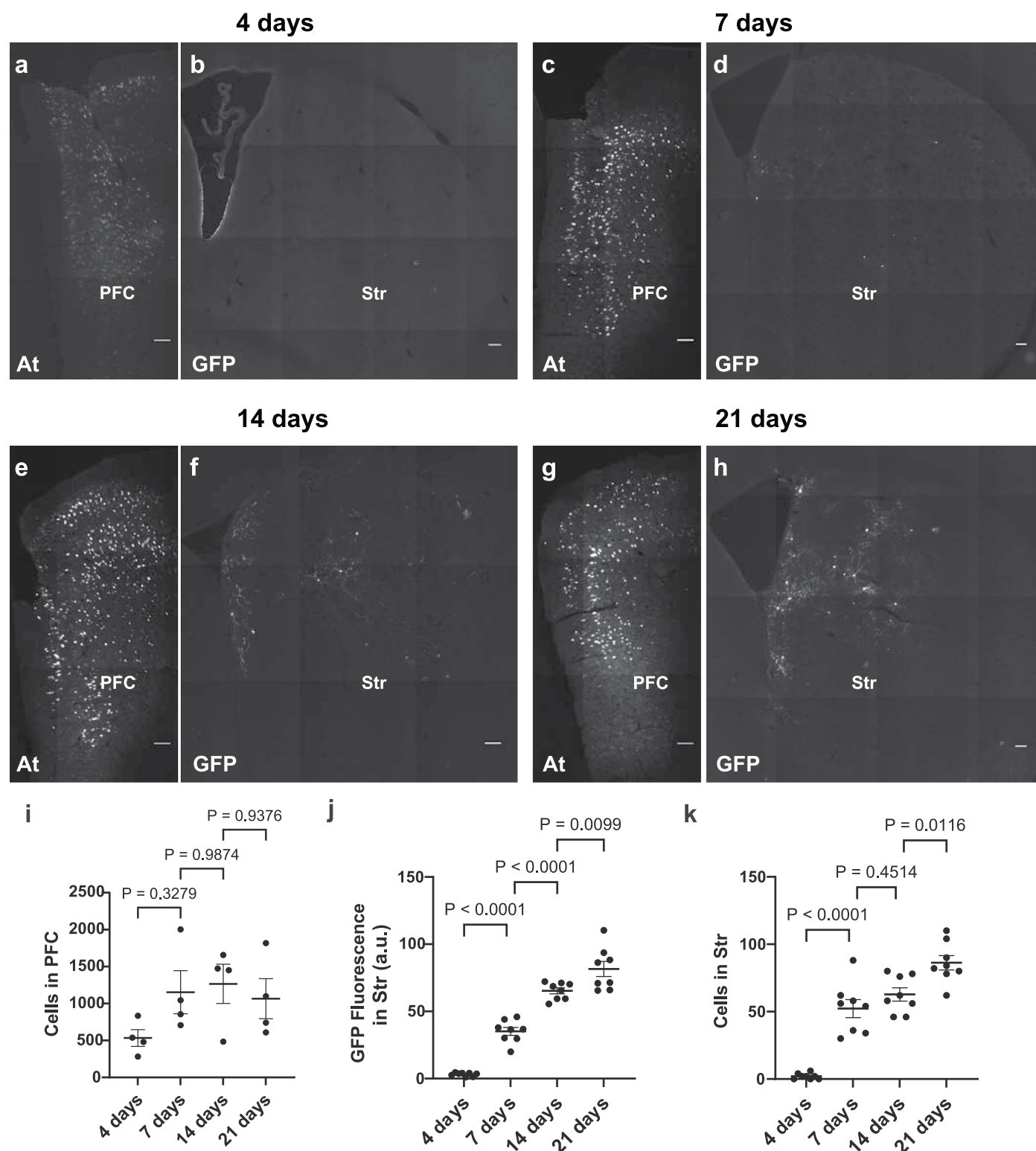
level of the thalamus of the same mouse brain as in **c.** and **d.** showing projections of neurons expressing BACE-GFP (green), neurons expressing mCherry (red) and Nissl stain (blue). **f.** Closeup of area marked in **e.** showing overlap of projections from neurons expressing AAV8-BACE-GFP (green) and neurons expressing mCherry. **g.** Coronal section at the level of the striatum of a control mouse injected with AAV8-DIO-mCherry in the striatum in an identical manner to the mice in **c.-f.** but with no injections in the cortex. Negligible mCherry labeling (red) is visible in the striatum. Sections were also stained with Nissl stain (blue). **h.** Closeup of area marked in **g.** showing negligible mCherry labeling. Scale bars in **a, b, d, f,** and **h** 100 μ m; in **c, e,** and **g** 1 mm.



Extended Data Fig. 8 | See next page for caption.

Extended Data Fig. 8 | Transsynaptic labeling of ATLASsn_{Cre} from cortical to subcortical areas. **a.** Coronal section from auditory cortex (A1) of a mouse injected with AAV8-ATLASsn_{Cre} and AAV8-BACE-HA in A1, and AAV8-DIO-GFP in bilateral inferior colliculi (IC) and incubated for two weeks showing At labeling of presynaptic neurons. **b.** Coronal section from the same mouse as in **a.** showing GFP labeling in bilateral IC consistent with bilateral postsynaptic staining. **c.** Closeup of area marked in **b.** **d.** Coronal section from prefrontal cortex of a mouse injected with AAV8-ATLASsn_{Cre} and AAV8-BACE-HA in the prefrontal cortex, and AAV8-DIO-GFP in the claustrum (Cl) and incubated for two weeks showing At labeling of presynaptic neurons. **e.** Coronal section from the same mouse as in **d.** showing GFP labeling in Cl. **f.** Closeup of area marked in **e.**

g. Horizontal section from entorhinal cortex of a mouse injected with AAV8-ATLASsn_{Cre} and AAV8-BACE-HA in the entorhinal cortex (EC), and AAV8-DIO-GFP in the hippocampus, and incubated for two weeks showing At labeling of presynaptic neurons. **h.** Horizontal section from the same mouse as in **g.** showing GFP labeling of dentate granule cells in the dentate gyrus (DG) and cells in the subiculum (Sub). **i.** Closeup of area marked in **h.** **j.** Quantitation of labeling of anterograde pathways. PFC-STR, Extended Data Fig. 3; PFC-CL, Extended Data Fig. 8d–f; A1-IC, Extended Data Fig. 8a–c; EC-Hp, Extended Data Fig. 8g–i; SC-PBG, Fig. 5j–l; LGN-V1, Fig. 3i–l; V1-SC, Fig. 3e–h. Each data point represents a biological replicate in a different mouse. Error bars depict mean \pm SEM. Scale bars 100 μ m.



Extended Data Fig. 9 | Time course of transsynaptic tracing from mPFC to striatum. **a.** Coronal section from PFC of a mouse injected with AAV8-ATLASn_{Cre} and AAV8-BACE-HA in PFC, and AAV8-DIO-GFP in Str, and incubated for four days. **b.** Coronal section from the same mouse as in **a.** **c.** Coronal section from PFC of an experiment similar to that in **a.** incubated for 7 days. **d.** Coronal section of Str from the same mouse as in **c.** **e.** Coronal section from PFC of an experiment similar to that in **a.** and **c.** incubated for 14 days. **f.** Coronal section of Str from

the same mouse as in **e.** **g.** Coronal section from PFC of an experiment similar to that in **a.**, **c.**, and **e.** incubated for 21 days. **h.** Coronal section of striatum from the same mouse as in **g.** **i.** The number of cells labeled in the PFC between 4 days and 21 days. **j.** The total intensity of GFP labeling in Str between 4 and 21 days. **k.** The number of cells labeled with GFP in Str between 4 and 21 days. Each data point represents a biological replicate in a different mouse. Scale bars 100 μ m.

Reporting Summary

Nature Portfolio wishes to improve the reproducibility of the work that we publish. This form provides structure for consistency and transparency in reporting. For further information on Nature Portfolio policies, see our [Editorial Policies](#) and the [Editorial Policy Checklist](#).

Statistics

For all statistical analyses, confirm that the following items are present in the figure legend, table legend, main text, or Methods section.

n/a	Confirmed
<input type="checkbox"/>	<input checked="" type="checkbox"/> The exact sample size (<i>n</i>) for each experimental group/condition, given as a discrete number and unit of measurement
<input type="checkbox"/>	<input checked="" type="checkbox"/> A statement on whether measurements were taken from distinct samples or whether the same sample was measured repeatedly
<input type="checkbox"/>	<input checked="" type="checkbox"/> The statistical test(s) used AND whether they are one- or two-sided <i>Only common tests should be described solely by name; describe more complex techniques in the Methods section.</i>
<input type="checkbox"/>	<input checked="" type="checkbox"/> A description of all covariates tested
<input type="checkbox"/>	<input checked="" type="checkbox"/> A description of any assumptions or corrections, such as tests of normality and adjustment for multiple comparisons
<input type="checkbox"/>	<input checked="" type="checkbox"/> A full description of the statistical parameters including central tendency (e.g. means) or other basic estimates (e.g. regression coefficient) AND variation (e.g. standard deviation) or associated estimates of uncertainty (e.g. confidence intervals)
<input type="checkbox"/>	<input checked="" type="checkbox"/> For null hypothesis testing, the test statistic (e.g. <i>F</i> , <i>t</i> , <i>r</i>) with confidence intervals, effect sizes, degrees of freedom and <i>P</i> value noted <i>Give P values as exact values whenever suitable.</i>
<input checked="" type="checkbox"/>	<input type="checkbox"/> For Bayesian analysis, information on the choice of priors and Markov chain Monte Carlo settings
<input checked="" type="checkbox"/>	<input type="checkbox"/> For hierarchical and complex designs, identification of the appropriate level for tests and full reporting of outcomes
<input checked="" type="checkbox"/>	<input type="checkbox"/> Estimates of effect sizes (e.g. Cohen's <i>d</i> , Pearson's <i>r</i>), indicating how they were calculated

Our web collection on [statistics for biologists](#) contains articles on many of the points above.

Software and code

Policy information about [availability of computer code](#)

Data collection	Slidebook 8 (3i), Zen Microscopy 3.11, NeuroLucida 360, NIS-Elements C6.10.01, GraphPad Prism 10.
Data analysis	Igor pro 9, NeuroInfo Version 2022.1.1, Matlab 2024a

For manuscripts utilizing custom algorithms or software that are central to the research but not yet described in published literature, software must be made available to editors and reviewers. We strongly encourage code deposition in a community repository (e.g. GitHub). See the Nature Portfolio [guidelines for submitting code & software](#) for further information.

Data

Policy information about [availability of data](#)

All manuscripts must include a [data availability statement](#). This statement should provide the following information, where applicable:

- Accession codes, unique identifiers, or web links for publicly available datasets
- A description of any restrictions on data availability
- For clinical datasets or third party data, please ensure that the statement adheres to our [policy](#)

All quantitative data in graphs and plots in Figs. 1-6 and Extended Data Figs. 1-9 are available in source files. Images used in quantifying transsynaptic experiments are available on the G-Node database https://gin.g-node.org/Haoyangh/ATLAS_nature_method_2024.git. All original microscopic images are available upon request to the corresponding author. AAV8-ATLASnCre, AAV8-DIO-ATLASnFlp, and AAV-DIO-BACE-HA sequences and plasmids are available at Addgene.

Human research participants

Policy information about [studies involving human research participants and Sex and Gender in Research](#).

Reporting on sex and gender	<input type="text" value="n/a"/>
Population characteristics	<input type="text" value="n/a"/>
Recruitment	<input type="text" value="n/a"/>
Ethics oversight	<input type="text" value="n/a"/>

Note that full information on the approval of the study protocol must also be provided in the manuscript.

Field-specific reporting

Please select the one below that is the best fit for your research. If you are not sure, read the appropriate sections before making your selection.

☒ Life sciences ☐ Behavioural & social sciences ☐ Ecological, evolutionary & environmental sciences

For a reference copy of the document with all sections, see [nature.com/documents/nr-reporting-summary-flat.pdf](https://www.nature.com/documents/nr-reporting-summary-flat.pdf)

Life sciences study design

All studies must disclose on these points even when the disclosure is negative.

Sample size	<input type="text" value="No sample size calculation was made. Sample size was based on prior studies in which similar analysis was performed (Zingg et al., 2017)."/>
Data exclusions	<input type="text" value="No data was excluded"/>
Replication	<input type="text" value="All data was replicated at least once."/>
Randomization	<input type="text" value="Animals were randomized. Experiments on tissue culture cells had controls performed in the same cultures"/>
Blinding	<input type="text" value="Blinding was not possible due to telltale signs that a particular experiment was a control or not, such as the presence or absence of At staining."/>

Reporting for specific materials, systems and methods

We require information from authors about some types of materials, experimental systems and methods used in many studies. Here, indicate whether each material, system or method listed is relevant to your study. If you are not sure if a list item applies to your research, read the appropriate section before selecting a response.

Materials & experimental systems

n/a	<input type="checkbox"/> Involved in the study
<input type="checkbox"/>	<input checked="" type="checkbox"/> Antibodies
<input type="checkbox"/>	<input checked="" type="checkbox"/> Eukaryotic cell lines
<input checked="" type="checkbox"/>	<input type="checkbox"/> Palaeontology and archaeology
<input type="checkbox"/>	<input checked="" type="checkbox"/> Animals and other organisms
<input checked="" type="checkbox"/>	<input type="checkbox"/> Clinical data
<input checked="" type="checkbox"/>	<input type="checkbox"/> Dual use research of concern

Methods

n/a	<input type="checkbox"/> Involved in the study
<input checked="" type="checkbox"/>	<input type="checkbox"/> ChIP-seq
<input checked="" type="checkbox"/>	<input type="checkbox"/> Flow cytometry
<input checked="" type="checkbox"/>	<input type="checkbox"/> MRI-based neuroimaging

Antibodies

Antibodies used	<input "="" type="text" value="Chicken anti-GFP, AVES (gfp-1020, NC9510598), 1:1000; Fluotag-X2 anti-ALFA, NanoTag (N1502-ALFA647-L), 1:1000; mouse anti-NeuN antibody, EMD Millipore (MAB377), 1:1000; c-Fos (9F6) Rabbit mAb, Cell Signalling Technology (2250T), 1:1000; rat anti-mCherry, Thermo Fisher (M112117, clone 16D7), 1:1000; Rabbit anti-RFP (1:2000, Rockland Inc., Limerick, PA, USA; Catalog #:600-401-379; Clonality: Polyclonal), Rabbit anti-GluA1, EMD Millipore (ABN241); mouse anti-PSD-95, NeuroMab (75-348, clone K28/74); mouse anti-Cre, EMD Millipore (MAB3120, clone 2D8), 1:1000; chicken anti-MYC, Novus Biologicals (NB600-334), 1:1000; Alexa Flour 488-conjugated goat anti-chicken Thermo Fisher (A11006), 1:1000; Alexa Flour 488-conjugated goat anti-mouse IgG,"/>
-----------------	----------------------------------------------------------------------------------------------------------------------------------------------------------------------------------------------------------------------------------------------------------------------------------------------------------------------------------------------------------------------------------------------------------------------------------------------------------------------------------------------------------------------------------------------------------------------------------------------------------------------------------------------------------------------------------------------------------------------------------------------------------------------------------------------------------

Thermo Fisher (A-11001), 1:1000; Alexa Flour 594-conjugated anti-rabbit IgG, Thermo Fisher (A-11012), 1:1000; Alexa Flour 594-conjugated anti-mouse IgG, Thermo Fisher (A-11005), 1:1000; Alexa Flour 647-conjugated goat anti-mouse IgG, Thermo Fisher (A-21235), 1:1000; Alexa Flour 647-conjugated goat anti-rabbit IgG, Thermo Fisher (A-21244), 1:1000;

Validation

all antibodies against tag peptides/proteins (GFP, RFP, anti-ALFA) were tested on neurons with and without the tag/peptide expressed to determine whether there were any off-target effects. Anti-Neun was validated in over 20 studies listed at https://www.merckmillipore.com/IE/en/product/Anti-NeuN-Antibody-clone-A60,MM_NF-MAB377?ReferrerURL=https%3A%2F%2Fwww.google.com%2F&bd=1#documentation. anti-c-fos was validated by western blot and 1103 citations at <https://www.cellsignal.com/products/primary-antibodies/c-fos-9f6-rabbit-mab/2250?srsltid=AfmBOoqNLE9a7fKDYaKHv1NlinKeVq7MTqpBwijJ5YVCUr2pKCoex8m>. anti-GluA1 was validated by immunocytochemistry and western blot at https://www.emdmillipore.com/US/en/product/Anti-GluR1-Antibody,MM_NF-ABN241. anti-PSD-95 was validated by immunocytochemistry and western blot on knockout animals at https://neuromab.ucdavis.edu/datasheet/K28_74.pdf. Anti-cre was validated with immunocytochemistry and references were listed at https://www.emdmillipore.com/US/en/product/Anti-Cre-Recombinase-Antibody-clone-2D8,MM_NF-MAB3120#documentation

Eukaryotic cell lines

Policy information about [cell lines and Sex and Gender in Research](#)

Cell line source(s)

COS7 cells (ATCC, CRL-1651). HEK 293T cells (ATCC, CRL-3216)

Authentication

cells were authenticated via morphological examination.

Mycoplasma contamination

cells were tested for mycoplasma by the supplier https://www.atcc.org/products/crl-1651?matchtype=b&network=g&device=c&adposition=&keyword=cos%207%20cells&gad_source=1&gclid=CjwKCAiApsm7BhBZEiwAvlu2X-Vdqp2d6x7x4Kjx5u4A1v9R-DfS8uFAzpkTFkT-wMgqFxRtZ_TsxoCTOMQAvD_BwE However, they were not independently tested in the investigator's lab.

Commonly misidentified lines (See [ICLAC](#) register)

n/a

Animals and other research organisms

Policy information about [studies involving animals; ARRIVE guidelines](#) recommended for reporting animal research, and [Sex and Gender in Research](#)

Laboratory animals

sprague dawley rats, P6-P8; C57BL/6J mice, 2-6 months; Vipr2-Cre (Cre expression in dLGN, Jackson Laboratories, strain #031332), and Sst-IRES-Cre (Cre expression in somatostatin interneurons, Jackson Laboratories strain #013044) mice aged 2–6 months. Mice and rats were housed in a light-controlled (12 h light/dark cycle) environment with ad libitum access to food and water. Ambient temperatures of 65-75 Deg F with 40-60% humidity were maintained for all animals.

Wild animals

n/a

Reporting on sex

Both sexes were used in all experiments. Sex-based data was not collected because there was no apparent variation with sex.

Field-collected samples

n/a

Ethics oversight

All experiments were performed in accordance with NIH Guidelines for the Care and Use of Laboratory Animals, and all procedures were approved by the Institutional Animal Care and Use Committee of the University of Southern California, NIH, or Harvard Medical School.

Note that full information on the approval of the study protocol must also be provided in the manuscript.